



OPEN ACCESS

EDITED BY

Yannick Poitelon,
Albany Medical College, United States

REVIEWED BY

Laura Fontenas,
Florida Atlantic University, United States
Ruth Martha Stassart,
Leipzig University, Germany

*CORRESPONDENCE

Peter Arthur-Farraj
✉ pja47@cam.ac.uk

†These authors have contributed equally to this work

‡These authors share senior authorship

SPECIALTY SECTION

This article was submitted to
Non-Neuronal Cells,
a section of the journal
Frontiers in Cellular Neuroscience

RECEIVED 03 February 2023

ACCEPTED 14 March 2023

PUBLISHED 05 April 2023

CITATION

Fazal SV, Mutschler C, Chen CZ, Turmaine M,
Chen C-Y, Hsueh Y-P, Ibañez-Grau A,
Loreto A, Casillas-Bajo A, Cabedo H,
Franklin RJM, Barker RA, Monk KR,
Steventon BJ, Coleman MP,
Gomez-Sanchez JA and Arthur-Farraj P (2023)
SARM1 detection in myelinating glia:
sarm1/Sarm1 is dispensable for PNS and CNS
myelination in zebrafish and mice.
Front. Cell. Neurosci. 17:1158388.
doi: 10.3389/fncel.2023.1158388

COPYRIGHT

© 2023 Fazal, Mutschler, Chen, Turmaine,
Chen, Hsueh, Ibañez-Grau, Loreto,
Casillas-Bajo, Cabedo, Franklin, Barker, Monk,
Steventon, Coleman, Gomez-Sanchez and
Arthur-Farraj. This is an open-access article
distributed under the terms of the [Creative Commons Attribution License \(CC BY\)](https://creativecommons.org/licenses/by/4.0/). The
use, distribution or reproduction in other
forums is permitted, provided the original
author(s) and the copyright owner(s) are
credited and that the original publication in this
journal is cited, in accordance with accepted
academic practice. No use, distribution or
reproduction is permitted which does not
comply with these terms.

SARM1 detection in myelinating glia: *sarm1/Sarm1* is dispensable for PNS and CNS myelination in zebrafish and mice

Shaline V. Fazal^{1,2†}, Clara Mutschler^{1†}, Civia Z. Chen²,
Mark Turmaine³, Chiung-Ya Chen⁴, Yi-Ping Hsueh⁴,
Andrea Ibañez-Grau⁵, Andrea Loreto¹, Angeles Casillas-Bajo^{5,6},
Hugo Cabedo^{5,6}, Robin J. M. Franklin^{2,7}, Roger A. Barker^{1,2},
Kelly R. Monk⁸, Benjamin J. Steventon⁹, Michael P. Coleman¹,
Jose A. Gomez-Sanchez^{5,6,10‡} and Peter Arthur-Farraj^{1**}

¹Department of Clinical Neurosciences, John van Geest Centre for Brain Repair, University of Cambridge, Cambridge, United Kingdom, ²Wellcome-MRC Cambridge Stem Cell Institute, University of Cambridge, Cambridge, United Kingdom, ³Department of Cell and Developmental Biology, University College London, London, United Kingdom, ⁴Institute of Molecular Biology, Academia Sinica, Taipei, Taiwan, ⁵Instituto de Neurociencias de Alicante, Universidad Miguel Hernández, Alicante, Spain, ⁶Instituto de Investigación Sanitaria y Biomédica de Alicante (ISABIAL), Alicante, Spain, ⁷Altos Labs - Cambridge Institute of Science, Cambridge, United Kingdom, ⁸Vollum Institute, Oregon Health & Science University, Portland, OR, United States, ⁹Department of Genetics, University of Cambridge, Cambridge, United Kingdom, ¹⁰Millennium Nucleus for the Study of Pain (MiNuSPain), Santiago, Chile

Since SARM1 mutations have been identified in human neurological disease, SARM1 inhibition has become an attractive therapeutic strategy to preserve axons in a variety of disorders of the peripheral (PNS) and central nervous system (CNS). While SARM1 has been extensively studied in neurons, it remains unknown whether SARM1 is present and functional in myelinating glia? This is an important question to address. Firstly, to identify whether SARM1 dysfunction in other cell types in the nervous system may contribute to neuropathology in SARM1 dependent diseases? Secondly, to ascertain whether therapies altering SARM1 function may have unintended deleterious impacts on PNS or CNS myelination? Surprisingly, we find that oligodendrocytes express *sarm1* mRNA in the zebrafish spinal cord and that SARM1 protein is readily detectable in rodent oligodendrocytes *in vitro* and *in vivo*. Furthermore, activation of endogenous SARM1 in cultured oligodendrocytes induces rapid cell death. In contrast, in peripheral glia, SARM1 protein is not detectable in Schwann cells and satellite glia *in vivo* and *sarm1/Sarm1* mRNA is detected at very low levels in Schwann cells, *in vivo*, in zebrafish and mouse. Application of specific SARM1 activators to cultured mouse Schwann cells does not induce cell death and nicotinamide adenine dinucleotide (NAD) levels remain unaltered suggesting Schwann cells likely contain no functionally relevant levels of SARM1. Finally, we address the question of whether SARM1 is required for myelination or myelin maintenance. In the

zebrafish and mouse PNS and CNS, we show that SARM1 is not required for initiation of myelination and myelin sheath maintenance is unaffected in the adult mouse nervous system. Thus, strategies to inhibit SARM1 function to treat neurological disease are unlikely to perturb myelination in humans.

KEYWORDS

Schwann cell, oligodendrocyte, myelination, SARM1, zebrafish, mouse

Introduction

The programmed axonal death (also termed Wallerian degeneration) pathway is becoming increasingly linked to neurological disease. Two of the most important regulators of this pathway are nicotinamide mononucleotide adenylyltransferase 2 (NMNAT2) and Sterile- α and Toll/interleukin 1 receptor (TIR) motif containing protein 1 (SARM1), a member of the MyoD88 family (Gilley and Coleman, 2010; Osterloh et al., 2012; Gerdtz et al., 2013; Coleman and Höke, 2020). Complete loss of function mutations in *Nmnat2* have been implicated in cases of fetal akinesia deformation sequence (FADS), where fetuses are stillborn with severe skeletal hypoplasia and hydrops fetalis, whereas partial loss of function mutations have been linked with the development of peripheral neuropathy with erythromelalgia (Huppke et al., 2019; Lukacs et al., 2019). The function of SARM1 in regulating axon degeneration is conserved between humans, mice and zebrafish and the *SARM1* locus has been identified in two Genome-wide association studies (GWAS) for Amyotrophic lateral sclerosis (ALS) (Osterloh et al., 2012; Fogh et al., 2014; van Rheenen et al., 2016; Tian et al., 2020; Chen et al., 2021). Following this, gain of function *SARM1* mutations have been identified in sporadic ALS and other motor nerve disorders (Gilley et al., 2021; Bloom et al., 2022). Additionally, the disused rat poison, vacor, which leads to highly specific activation of SARM1, causes severe neurotoxic effects in humans. (LeWitt, 1980; Loreto et al., 2021).

Axon dysfunction and loss are hallmarks of many neurological diseases of the central (CNS) and peripheral nervous system (PNS), including Parkinson disease, traumatic brain injury, progressive multiple sclerosis, ALS and the many inherited and acquired peripheral neuropathies (Coleman and Höke, 2020). *Sarm1* deletion has shown to have significant protective effects on axon loss in animal models of traumatic brain injury, metabolic neuropathy and several models of chemotherapy induced neuropathy (Geisler et al., 2016, 2019a; Henninger et al., 2016; Turkiew et al., 2017; Cheng et al., 2019; Marion et al., 2019; Bosanac et al., 2021; Gould et al., 2021b). Thus, inhibition or knockdown of SARM1 through use of pharmacological, gene therapy and antisense oligonucleotide approaches have become very attractive therapeutic strategies to trial in various neurological diseases (Geisler et al., 2019b; Coleman and Höke, 2020; Krauss et al., 2020; Arthur-Farraj and Coleman, 2021; Bosanac et al., 2021; Gould et al., 2021a; Merlini et al., 2022).

SARM1 is abundant in the nervous system but is not found in most other tissues, including heart, kidney, liver, lung, skeletal muscle, spleen or thymus (Kim et al., 2007; Chen et al., 2011). While neurons have been shown to have high levels of SARM1 it is

unknown whether it is also present in myelinating glia in the PNS or CNS. Furthermore, it remains undetermined, due to the lack of in-depth quantitative studies on myelination, whether SARM1 has any role in regulating oligodendrocyte or Schwann cell myelination or myelin maintenance in either a cell autonomous or non-cell autonomous fashion. This is important to know as it could have adverse implications for the use of therapies aimed to treat various neurological disorders through inhibition of SARM1 function.

In this study, we use mice and larval zebrafish to demonstrate that *Sarm1/sarm1* mRNA is present at low levels in developing Schwann cells but abundant in oligodendrocytes. In the adult murine nervous system, SARM1 protein is detectable in oligodendrocytes but not in Schwann cells and satellite glia. In cultured cells, use of the specific SARM1 activators, vacor and 3-acetylpyridine (3-AP) confirms that Schwann cells contain negligible amounts of SARM1 whereas cultured oligodendrocytes contain functionally relevant levels of SARM1 protein. Furthermore, we show that, in the absence of SARM1/*Sarm1*, myelination in the PNS and CNS is initiated in a timely fashion in both mice and larval zebrafish and that PNS and CNS myelin maintenance in adult mice is unaffected.

Results

SARM1 protein is present in oligodendrocytes but not in Schwann cells nor satellite glia

In order to investigate the presence of SARM1 protein in various cell types in the murine nervous system we used a validated polyclonal antibody generated by Chen et al. (2011) in transverse cryosections of adult (P60) tibial and optic nerve. As expected, we found that SARM1 expression colocalized with the axonal markers neurofilament and beta-III tubulin in sciatic and optic nerve respectively (Figures 1A, B). Additionally, we found that SARM1 protein was present ubiquitously, at high levels, in large and small dorsal root ganglion (DRG) neuron cell bodies, *in vivo*, compared to lower levels within their axons (Figure 1C). Importantly, we saw no staining in control sections without primary antibody nor in *Sarm1* knockout (KO) DRG neurons (Supplementary Figures 1A, B). To test if there were detectable levels of SARM1 protein in myelinating and non-myelinating Schwann cells, satellite glia and oligodendrocytes we performed SARM1 and SOX10 immunohistochemistry in cryosections from tibial nerves, DRGs and optic nerves. In PNS tissue we found no colocalization in multiple sections from 3

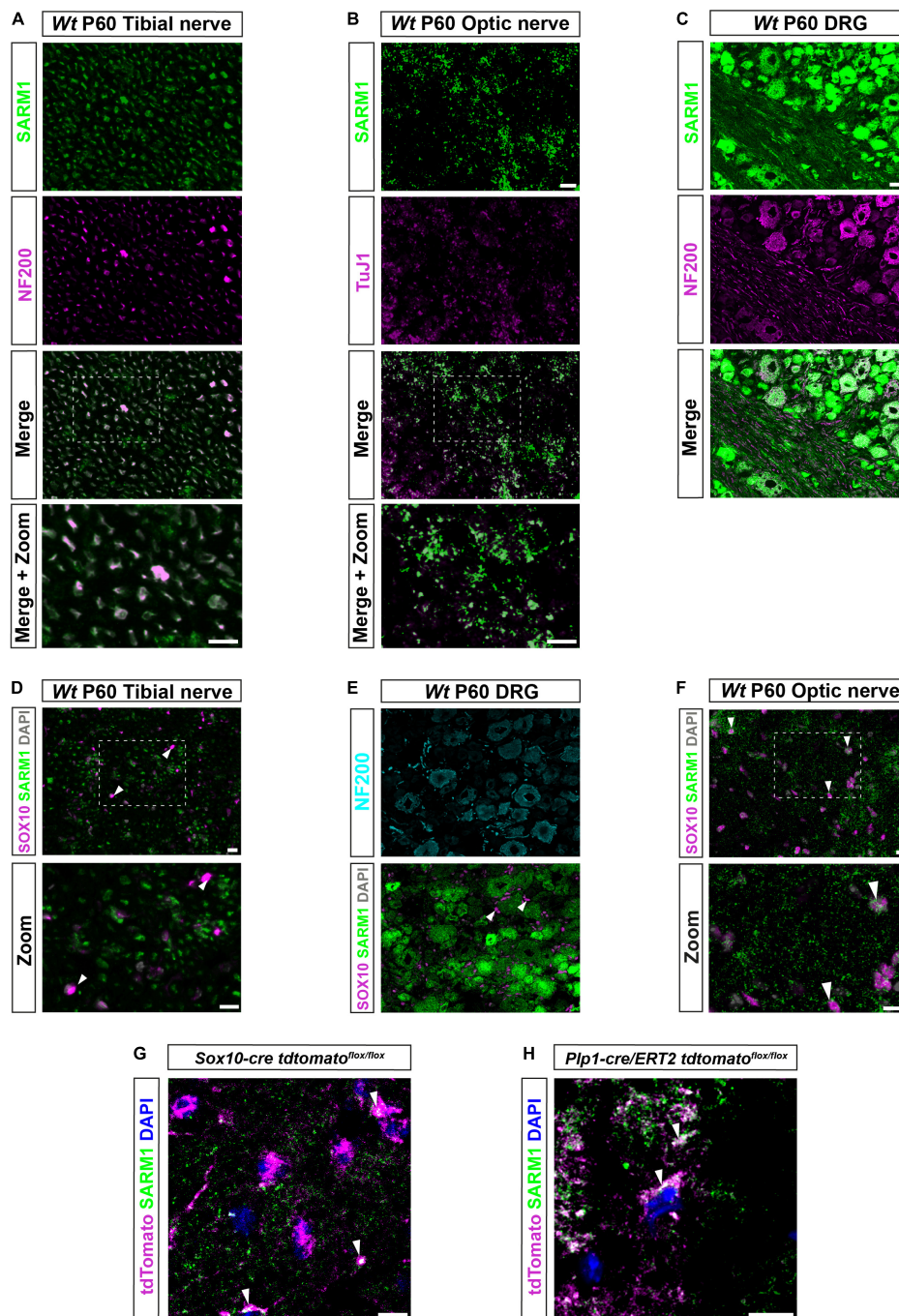


FIGURE 1

SARM1 protein is detectable in CNS myelinating glia but not PNS glia. **(A)** Representative immunofluorescence images of transverse sections of *Wt* mouse tibial nerves to show co-localization of SARM1 (green) and NF-200 (neurofilament light chain; magenta) in axons. Zoomed area is represented by the white bounding box. Scale bars 10 μm . **(B)** Representative immunofluorescence images of transverse sections of *Wt* mouse optic nerves to show expression of SARM1 (green) in TUJ1 (Anti-Beta III Tubulin; magenta) positive axons. Zoomed area is represented by the white bounding box. Scale bars 10 μm . **(C)** Representative immunofluorescence images of transverse sections of *Wt* mouse DRGs to show co-localization of SARM1 (green) and NF-200 (magenta) positive neurons. Scale bar 25 μm . **(D)** Representative immunofluorescence images of transverse sections of *Wt* and *Sarm1* KO mouse tibial nerves showing SARM1 (green) and SOX10 (magenta) expression. White arrowheads show co-localization of DAPI (gray) and SOX10 (magenta), but no expression of SARM1 (green). Zoomed areas are represented by the white bounding box. Scale bar 10 μm . **(E)** Representative immunofluorescence images of transverse sections of *Wt* and *Sarm1* KO mouse DRGs showing NF200 (cyan), SARM1 (green) and SOX10 (magenta) expression. White arrowheads point to SOX10 (magenta) positive satellite glia and DAPI (gray), with no colocalization of SARM1 (green). Scale bar 10 μm . **(F)** Representative immunofluorescence images of transverse sections of *Wt* and *Sarm1* KO mouse optic nerves showing SARM1 (green) and SOX10 (magenta) expression. White arrowheads point to SOX10 (magenta) positive oligodendrocytes and DAPI (gray), with perinuclear SARM1 staining (green). Scale bar 10 μm . Zoomed areas are represented by the white bounding box. Scale bar 10 μm . All experiments $n = 3$ (3 animals, 2 nerves per animal, 5 sections per nerve). **(G)** Maximum projection of tdTomato positive oligodendrocytes in P60 optic nerves of *Sox10-cre Rosa26 stopflox tdtomato* (*Sox10-cre tdtomato*^{*fllox/fllox*}) positive for SARM1 immunolabelling (white arrowhead). Scale bar 10 μm . **(H)** Single confocal z plane of tdTomato positive oligodendrocytes in P60 optic nerves of *Plp1-cre/ERT2 Rosa26 stopflox tdtomato* (*Plp1-cre/ERT2 tdtomato*^{*fllox/fllox*}) positive for SARM1 immunolabelling (white arrowhead). Scale bar 10 μm .

separate non-littermate animals (Figures 1D, E). However, in optic nerve sections SARM1 protein appeared present in a perinuclear staining pattern around SOX10 positive nuclei (Figure 1F). To confirm this, we performed SARM1 immunohistochemistry in optic nerves of two mutant mouse lines where oligodendrocytes are labeled with tdTomato; either *Plp1-cre/ERT2* or *Sox10-cre* mouse lines bred with homozygous *Rosa26 stopflox tdtomato* mice. In both lines, tdTomato positive cells contained SARM1 immunolabelling, including in single confocal slices (Figures 1G, H). Thus, SARM1 protein appears restricted to neuronal populations in the PNS and is not detectable in adult murine Schwann cells and satellite glia. However, in the adult mammalian CNS, SARM1 protein is readily detectable in oligodendrocytes.

To identify if *sarm1* mRNA is expressed in myelinating glia in zebrafish, we used third generation *in situ* hybridization chain reaction (HCR), in five-day post fertilization (5dpf) zebrafish larvae, where both oligodendrocytes and Schwann cells, in the CNS and PNS, respectively, are initiating myelination (D'Rozario et al., 2017; Choi et al., 2018). We used HCR probes targeted to *sarm1* and *sox10* to label cells of the oligodendrocyte and Schwann cell lineage. In the posterior lateral line nerve (PLLn) we saw strong expression of *sox10* but little *sarm1* expression, though importantly we saw no *sarm1* signal when antisense probes were omitted (Figure 2A and Supplementary Figures 2A, B). To investigate whether *sarm1* and *sox10* were co-expressed in the same cells in the PNS, we examined individual confocal slices (616nm optical thickness) and found that we could only see co-expression of both markers in nuclei along the PLLn infrequently (Figure 2B). Specifically, we found that $22.4\% \pm 3.161$ of Schwann cells, in the PLLn, express a low level of *sarm1*. In the spinal cord, while we saw *sox10* expression mainly concentrated in the ventral and dorsal spinal cord tracts, we visualized *sarm1* expression more diffusely throughout the whole spinal cord (Figure 2C). In single confocal slices, we found that $60.3\% \pm 2.4$ of *sox10* positive cells also expressed *sarm1* (Figure 2D).

In combination, these results are consistent with the view that peripheral glia such as Schwann cells and satellite glia do not contain detectable levels of SARM1, whereas oligodendrocytes in the CNS express substantial levels of *sarm1*/SARM1 in fish and mice.

Cultured oligodendrocytes, but not Schwann cells, have detectable SARM1 protein and are vulnerable to specific, SARM1 activator-induced cell death

Since we were unable to identify SARM1 protein in Schwann cells *in vivo* but we did find that a proportion of zebrafish Schwann cells express low levels of *Sarm1* mRNA, we wanted to further explore whether Schwann cells may contain small amounts of functional SARM1 protein below the threshold of antibody detection. Firstly, we confirmed that cultured mouse Schwann cells also express very low levels of *Sarm1* mRNA, similar to our finding in zebrafish larvae (Supplementary Figure 3A). Additionally, we were unable to detect SARM1 protein in Schwann cell cultures, using immunocytochemistry (Supplementary Figure 3B).

To test if Schwann cells have any functional SARM1 protein, we treated cultures of freshly isolated mouse Schwann cells with two separate SARM1 activators, vacor and 3-AP. Addition of high dose vacor (100 μ M) or 3-AP (250 μ M) to neuronal cultures induces rapid SARM1 activation, profound Nicotinamide adenine dinucleotide (NAD⁺) depletion and axonal degeneration and cell death within hours (Loreto et al., 2021; Wu et al., 2021). We found that mouse Schwann cells were completely insensitive to induction of cell death by both vacor and 3-AP treatment at high doses for long periods of time (up to 72 h) (Figure 3A and Supplementary Figure 4A). Furthermore, Schwann cells treated with vacor or 3-AP for 72 hours showed no reduction in intracellular NAD⁺ levels, unlike in Human embryonic kidney cells, which express low levels of SARM1 protein (Figure 3B and Supplementary Figure 4B). In contrast, we found that treatment of rat oligodendrocyte cultures with vacor induced cell death within hours, and complete loss of cultures after 72 h of treatment (Figures 3C, D). Predictably, when we immunolabelled oligodendrocyte cultures we found the presence of detectable levels of SARM1 using two different antibodies, in line with our *in vivo* findings (Figure 3E and Supplementary Figure 4C). Thus, cultured Schwann cells, in contrast to oligodendrocytes, do not contain sufficient endogenous SARM1 protein to induce either cell death or a decline in cellular NAD⁺ levels.

Initiation of CNS and PNS myelination proceeds normally in *sarm1* mutant zebrafish larvae

Since inhibition of SARM1 function is being proposed to treat neurological disease, it is crucial to identify whether loss of SARM1 leads to any disruption of vertebrate CNS or PNS myelination in a cell autonomous or non-cell autonomous fashion. This is especially important given we have now shown that oligodendrocytes contain functional SARM1 protein *in vitro* and *in vivo*. To date, no studies have performed an in-depth quantitative analysis of CNS and PNS myelination in the absence of SARM1 function. To test whether *Sarm1* is required for initiation of myelination in zebrafish we assessed myelination and myelin gene expression in the spinal cord and PLLn in *wild-type* (*wt*) and *sarm1*^{SA11193/SA11193} (mutant) larvae at 5dpf. The *sarm1*^{SA11193} mutants fish harbor a point mutation (C > A) in exon 2, which introduces a premature stop codon (Kettleborough et al., 2013). *sarm1*^{SA11193} mutants are viable, fertile and appear morphologically indistinct from *wt* fish (data not shown). To confirm that *sarm1* mutants behave functionally like *sarm1* null animals, which have substantially delayed axonal degeneration after traumatic injury, we injected *wt* and homozygous mutant fish with a *neuroD:tdTomato* DNA construct at the one-celled zygote stage. We then performed 2-photon laser axotomy of tdTomato labeled PLLn neurons at 4dpf and live imaged the axons distal to the injury site (Supplementary Figure 5A). We found that while *wt* axons started to degenerate between 2 h 40 min and 3 h 20 min ($n = 7$), axons in *sarm1* mutant fish remained intact even 26 h after axotomy, which was the limit of our imaging abilities due to UK home office regulations (Supplementary Figure 5B). This confirmed that *sarm1*^{SA11193} mutant zebrafish phenotypically behave like *Sarm1* null mice and

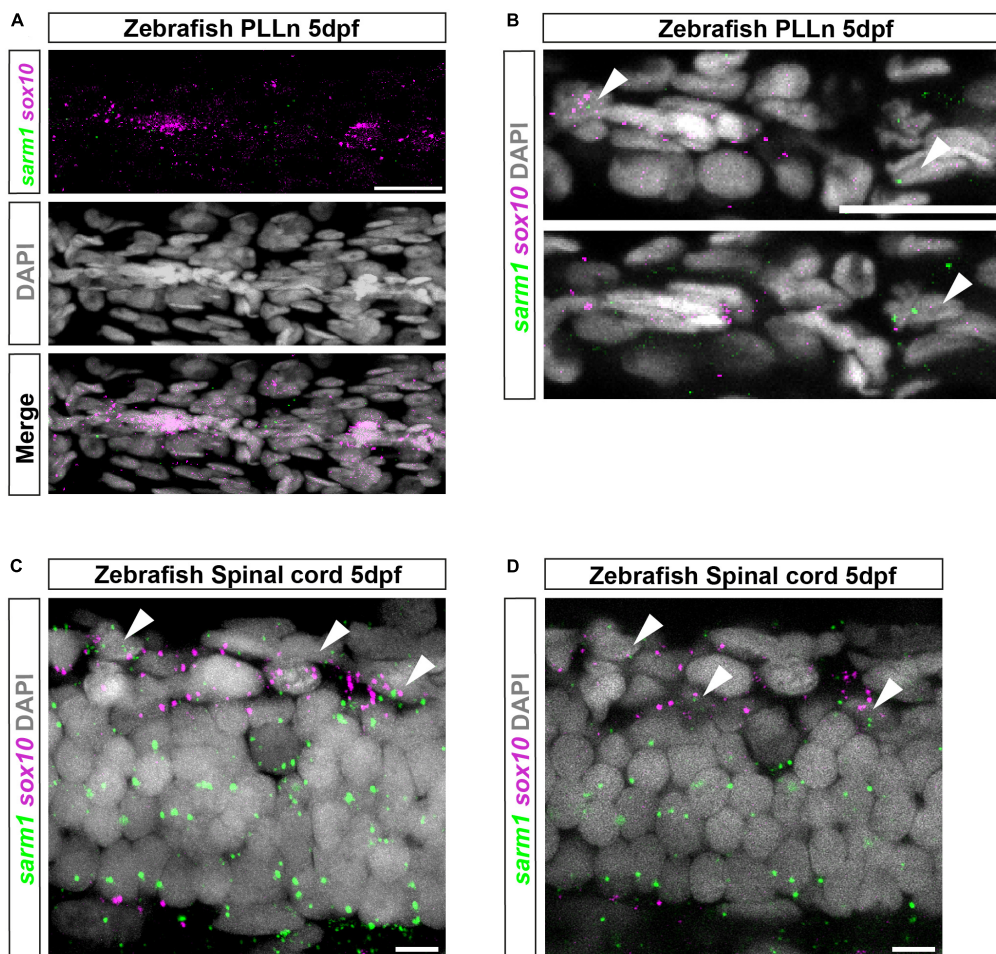


FIGURE 2

sarm1 expression in zebrafish larvae PLLn and spinal cord. (A) MAX projection, lateral view of PLLn of a 5dpf larva demonstrating HCR *in situ* labeling for *sox10* and *sarm1* mRNA and DAPI staining to mark nuclei. (B) Single confocal z plane, 616 nm optical thickness, lateral view of PLLn of a 5dpf larva. Arrowheads mark nuclei, labeled with DAPI, positive for *sox10* and *sarm1* mRNA. In the PLLn, $22.4\% \pm 3.161$ [mean and standard error of mean (SEM), $n = 5$ larvae, 5 sections per larvae] of *sox10* positive cells also expressed *sarm1*. (C) MAX projection, lateral view of spinal cord of a 5dpf larva demonstrating HCR *in situ* labeling for *sox10* and *sarm1* mRNA and DAPI staining to mark nuclei. Arrowheads mark nuclei positive for *sox10* and *sarm1* mRNA. (D) Single confocal z plane, 475 nm optical thickness, lateral view of spinal cord of a 5dpf larva. Arrowheads mark nuclei positive for *sox10* and *sarm1* mRNA. In the spinal cord, $60.3\% \pm 2.4$ (mean and SEM, $n = 5$ larvae, 3 sections quantified per larvae) of *sox10* positive cells also expressed *sarm1*. For all images: *sox10* mRNA (magenta) and *sarm1* mRNA (green), nuclei labeled with DAPI (gray), scale bar 25 μm .

are similar to a Crispr-Cas9 generated *sarm1* null mutant zebrafish (Tian et al., 2020).

To assess PNS and CNS myelination, we next crossed *sarm1*^{SA11193} mutants with *Tg(mbp:EGFP-CAAX)* zebrafish that express membrane bound GFP under the myelin basic protein (*mbp*) promoter. Since the GFP is membrane bound, GFP intensity acts as a surrogate marker for myelin membrane formation (Almeida et al., 2011). We observed normal formation of long GFP-labeled myelin segments in the dorsal and ventral spinal cord as well as PLLn in both 5dpf *sarm1*^{SA11193} mutants and *wt* fish and quantification showed no differences in PLLn and spinal cord myelination (Figures 4A-F).

Additionally, we quantified myelin gene expression in the PLLn between *wt* and *sarm1* mutant zebrafish using *mbp* HCR. We found that there were equivalent levels of total *mbp* expression in the PLLn in *wt* and *sarm1*^{SA11193} mutant fish and importantly, there were no differences in cell numbers between genotypes (Figures 4G-I).

Collectively these experiments demonstrate that myelination proceeds normally in both the PLLn and spinal cord in zebrafish larvae in the absence of Sarm1 function.

PNS myelination and myelin maintenance are normal in the *Sarm1* KO mouse

Given that zebrafish embryos appear to myelinate normally without functional Sarm1, we next tested whether PNS myelination in *Sarm1* KO mice is initiated on time. PNS myelination starts shortly after birth in murine peripheral nerves (Jessen and Mirsky, 2005). We looked at postnatal (P) day 2 transverse sections through the sciatic nerve by transmission electron microscopy (EM) and noted that while there was a non-significant trend toward slightly more axons and Schwann cells in the *Sarm1* KO nerves

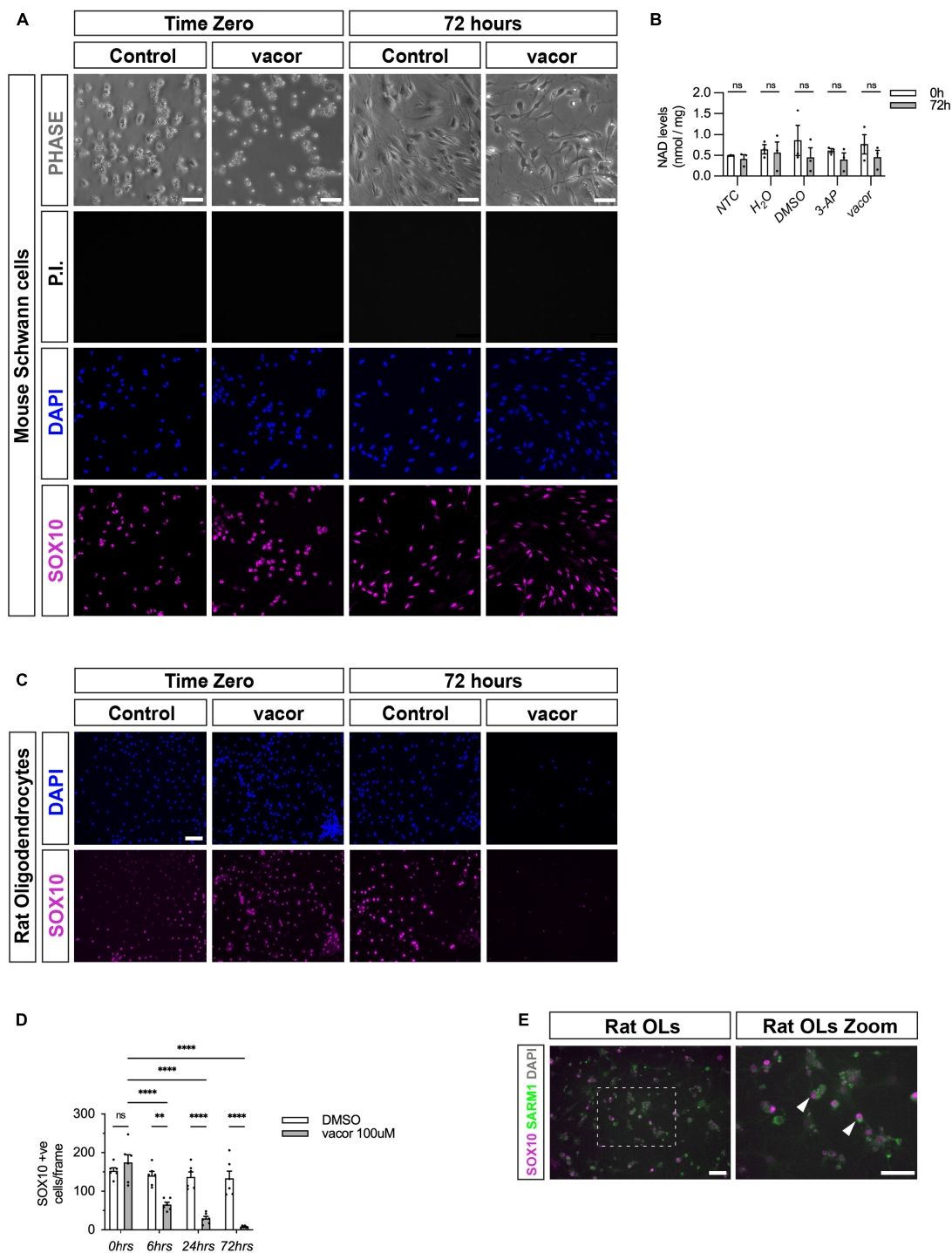


FIGURE 3

Cultured oligodendrocytes, but not Schwann cells, are sensitive to specific SARM1 activators. **(A)** Dissociated and freshly plated P2 mouse Schwann cells cultured in DMSO or 100 μ M vacor for 72 h show no cell death, judged by propidium iodide (P.I.) and DAPI nuclear staining and SOX10 immunocytochemistry. $96.4\% \pm 0.3$ SOX10 positive cells survived after 72 h 100 μ M vacor treatment (mean and SEM, $n = 3$: two-four mice, each from three litters producing three separate cultures, $p = 0.53$). **(B)** Intracellular NAD⁺ levels do not change in Schwann cells when treated for 72 h with either 250 μ M 3-AP (mean and SEM of Time zero (TZ) 0.61 ± 0.05 and 72 h 0.4 ± 1.15 , $n = 3$, $p = 0.63$) or 100 μ M vacor (mean and SEM of TZ 0.76 ± 0.23 and 72 h 0.46 ± 0.16 , $n = 3$, $p = 0.63$) compared to control conditions (mean and SEM of H₂O: TZ 0.64 ± 0.1 , 72 h 0.56 ± 0.25 , $n = 3$, $p = 0.81$; mean and SEM of DMSO: TZ 0.85 ± 0.36 , 72 h 0.45 ± 0.22 , $n = 3$, $p = 0.61$). **(C)** Rat oligodendrocytes cultured in DMSO or 100 μ M vacor for 72 h demonstrate substantial cell death judged by DAPI nuclear staining and SOX10 immunocytochemistry ($n = 5$: one rat from five litters producing five separate cultures). Scale bar 50 μ m. **(D)** Quantification of SOX10 positive oligodendrocyte cell survival in response to 100 μ M vacor treatment compared to DMSO control cultures. After six, 24 and 72 h of 100 μ M vacor treatment, $47.9\% \pm 6.5$, $21.6\% \pm 4.5$ and $6.5\% \pm 1.2$ of SOX10 expressing cells survived respectively (mean and SEM, $n = 5$, $p = 0.02$, $p < 0.0001$, $p < 0.0001$ respectively). **(E)** Cultured rat oligodendrocytes (OLs; SOX10 positive) contain substantial SARM1 protein using a polyclonal anti-SARM1 antibody generated by Y-PH. Zoomed in area (indicated by dashed box). Arrowheads indicate SOX10 positive SARM1 positive cells. Scale bars 50 μ m. ** $P < 0.01$, **** $P < 0.0001$.

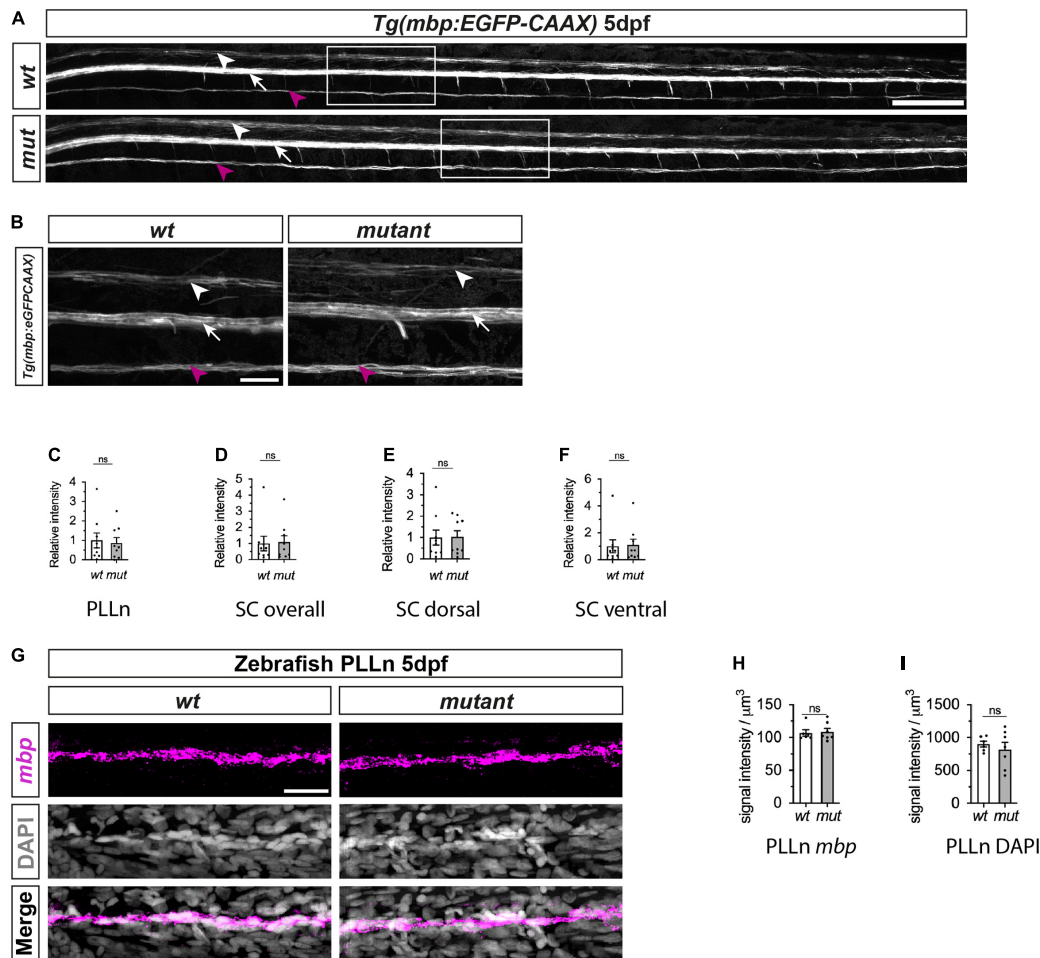


FIGURE 4

Myelination of PLLn and spinal cord is unaffected by absence of functional *Sarm1* in zebrafish. (A) Max projection of the lateral view of wild-type (*wt*) *Tg(mbp:EGFP-CAAX)* and *sarm1*^{SA11193/SA11193} (*sarm1* mutant, *mut*) *Tg(mbp:EGFP-CAAX)* 5 dpf larva. Arrowhead (white) delineates the dorsal spinal cord; Arrow (white) marks the ventral spinal cord; Arrow (magenta) pinpoints the PLLn. Scale bar 100 μm . (B) Zoomed in lateral view of spinal cord and PLLn (area indicated by boxes in A). Arrowhead (white) delineates the dorsal spinal cord; Arrow (white) marks the ventral spinal cord; Arrow (magenta). Scale bar 25 μm . (C) Relative intensity of GFP in PLLn of *Tg(mbp:EGFP-CAAX)* *wt*, 1.0 ± 0.38 and *sarm1* mutant (*mut*), 0.86 ± 0.28 (mean and SEM, $n = 9$; $p = 0.8633$). (D) Relative intensity of GFP in the dorsal and ventral spinal cord combined of *Tg(mbp:EGFP-CAAX)* *wt*, 1.0 ± 0.44 and *sarm1* mutant (*mut*), 1.08 ± 0.38 (*mut*) (mean and SEM, $n = 9$; $p = 0.8633$). (E) Relative intensity of GFP in the dorsal spinal cord of *Tg(mbp:EGFP-CAAX)* *wt*, 1.0 ± 0.35 and *sarm1* mutant (*mut*), 1.03 ± 0.28 (mean and SEM, $n = 9$; $p = 0.9314$). (F) Relative intensity of GFP in the ventral spinal cord of *Tg(mbp:EGFP-CAAX)* *wt*, 1.0 ± 0.48 and *sarm1* mutant (*mut*), 1.1 ± 0.44 (mean and SEM, $n = 9$; $p = 0.8633$). (G) MAX projection, lateral view of PLLn of *wt* and *sarm1* mutant (*mutant*) 5 dpf larvae showing *mbp* (magenta) mRNA expression. Nuclei labeled with DAPI (gray). Scale bar 25 μm . (H) Quantification of *mbp* mRNA signal intensity/ μm in PLLn of *wt*, 107.0 ± 4.72 and *sarm1* mutant, 108.82 ± 5.14 (*mut*) 5 dpf larvae (mean and SEM, WT $n = 6$; MUT $n = 7$; $p = 0.8357$). (I) Quantification of DAPI signal intensity/ μm in PLLn of *wt*, 902.5 ± 45.2 and *sarm1* mutant (*mut*), 822 ± 108.77 , 5 dpf larvae (mean and SEM, WT $n = 6$; MUT $n = 7$; $p = 0.7308$).

compared to *Wt* ($n = 5$), there was no difference in the proportion of large caliber axons that were myelinated (Figures 5A–G and Supplementary Figure 5C). We then looked at adult (P60) sciatic nerves by EM to investigate whether myelin maintenance is affected by loss of *Sarm1* in the PNS. Interestingly we no longer saw a trend toward increased axon numbers in the *Sarm1* KO at P60 (Figures 5H–I). Furthermore, the proportion of unmyelinated and myelinated axons, Schwann cell nuclei as well as myelin sheath thickness, measured by g-ratio and nerve area were all similar between *Wt* and *Sarm1* KO samples (Figures 5M, N and Supplementary Figure 5D). Interestingly, when we plotted g-ratio against axon caliber there appear to be a subtle trend toward large caliber axons demonstrating a slightly lower g-ratio. However, on direct comparison of axons with a calibre $> 10 \mu\text{m}$ between *Wt*

(0.72 ± 0.004) and *Sarm1* KO (0.73 ± 0.004) mice, we saw no statistical difference ($n = 4$, $p = 0.2857$) (Figures 5O, P).

To test whether there were any gene expression differences between *Wt* and *Sarm1* KO nerves we looked at gene and protein expression by quantitative reverse transcriptase polymerase chain reaction (qPCR) and western blot respectively in pooled tibial nerves. *Sarm1* KO nerves had no differences in myelin gene or other Schwann cell-specific gene expression (*Cdh1*, *Egr2*, *Mbp*, *Mpz*, *Sox10*), immature or Schwann cell injury gene expression (*Fos*, *Jun*, *Sox2*) or cytokine or chemokine expression (*Ccl2*, *Ccl3*, *Ccl4*, *Ccl5*, *Il1b*, *IL6*, *IL10*). We did however detect that *Sarm1* KO tibial nerves expressed a two-fold higher level of the pro-apoptotic gene, *Xaf1*, which has also been reported to be upregulated in mouse brain and macrophages from this particular *Sarm1* KO mouse line

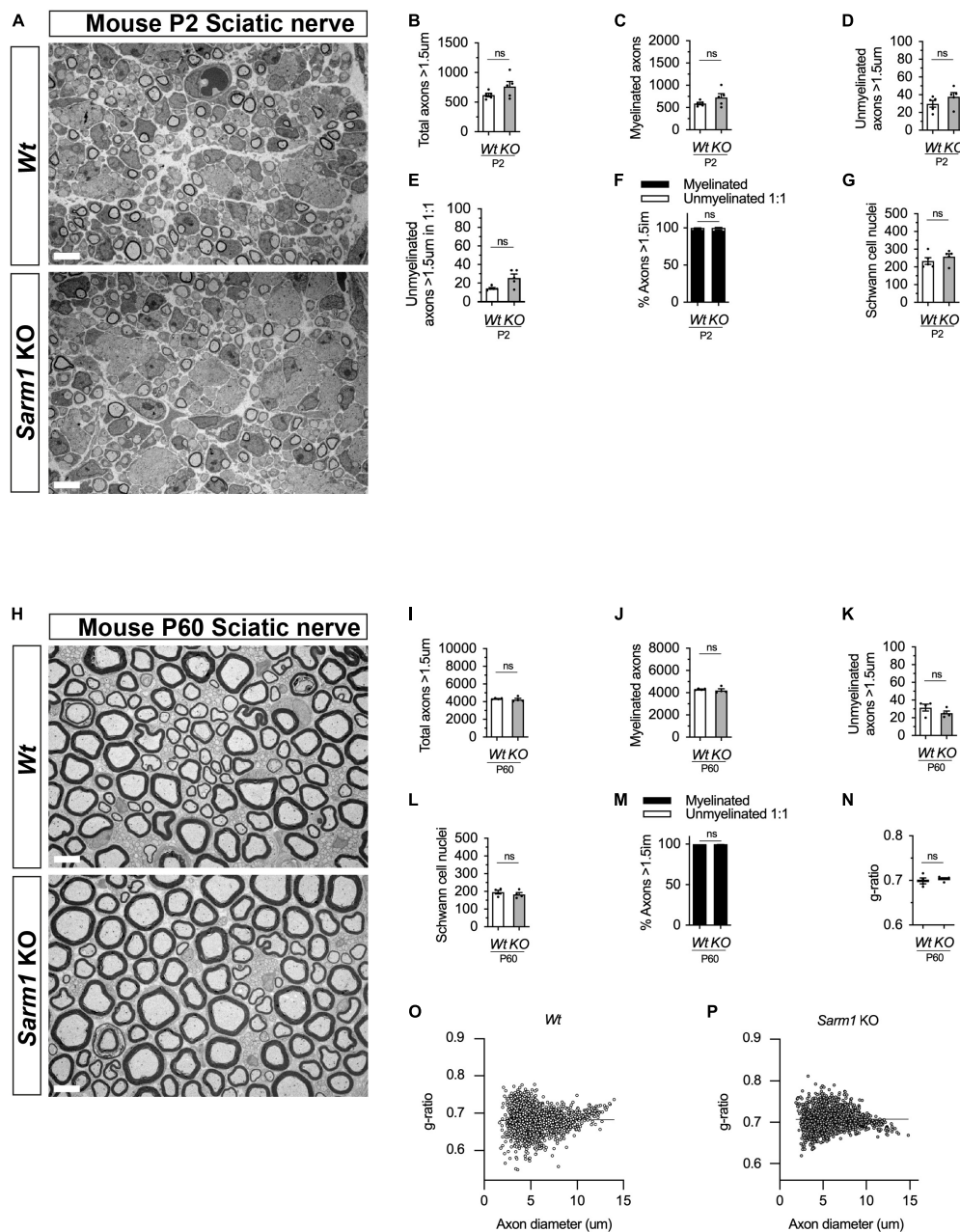


FIGURE 5

PNS myelination and myelin maintenance are normal in *Sarm1* null mice. (A) Representative electron micrographs taken at $\times 3,000$ magnification from *Wt* and *Sarm1* knockout (KO) sciatic nerves at postnatal day 2 (P2). Scale bar $5 \mu\text{m}$. (B) Per nerve profile, the total number of axons $> 1.5 \mu\text{m}$ quantified are not significantly different in *Wt*, 621.0 ± 28.99 , and *Sarm1* KO, 763.0 ± 86.35 , nerves (mean and SEM, $n = 5$; $p = 0.3095$). (C) The number of myelinated axons quantified per nerve profile are similar in both *Wt*, 591.2 ± 26.67 , and *Sarm1* KO, 725.0 ± 86.37 , nerves (mean and SEM, $n = 5$; $p = 0.3095$). (D) The number of unmyelinated axons $> 1.5 \mu\text{m}$ is not significantly different in *Wt*, 29.8 ± 3.77 , and *Sarm1* KO, 37.8 ± 4.73 , nerves (mean and SEM, $n = 5$; $p = 0.1508$). (E) Per nerve profile, the number of unmyelinated axons $> 1.5 \mu\text{m}$ in a ratio 1:1 is slightly higher in *Sarm1* KO, 25.8 ± 3.96 , nerves compared to *Wt*, 14.4 ± 0.98 ; however, this does not reach significance (mean and SEM, $n = 5$; $p = 0.0873$). (F) The percentage of myelinated axons versus non-myelinated axons present in *Wt*, $97.63\% \pm 0.19$ and *Sarm1* KO, $96.4\% \pm 0.75$, nerves is not significantly different ($n = 5$; $p = 0.1508$). (G) The number of Schwann cell nuclei quantified per nerve profile is not significantly different between *Wt*, 234.0 ± 18.93 and *Sarm1* KO, 258.2 ± 16.79 nerves (mean and SEM, $n = 5$; $p = 0.5476$). (H) Representative electron micrographs taken at $\times 3000$ magnification from adult *Wt* and *Sarm1* KO sciatic nerves at P60. There are no ultrastructural differences in the sciatic nerves of adult *Sarm1* KO compared to those of *Wt* sciatic nerves. Scale bar $5 \mu\text{m}$. (I) Per nerve profile, the total number of axons $> 1.5 \mu\text{m}$ quantified is similar in *Wt*, 4341 ± 34.27 and *Sarm1* KO, 4241 ± 138.3 sciatic nerves (mean and SEM, $n = 4$; $p = 0.3429$). (J) The number of myelinated axons present in *Wt*, 4310 ± 31.37 and *Sarm1* KO, 4216 ± 136.2 nerves is not significantly different (mean and SEM, $n = 4$; $p = 0.3429$). (K) Per nerve profile, the number of unmyelinated axons $> 1.5 \mu\text{m}$ is not significantly different in *Wt*, 31.5 ± 3.86 and *Sarm1* KO, 25.25 ± 2.4 nerves (mean and SEM, $n = 4$; $p = 0.3429$). (L) The number of Schwann cell nuclei is similar in both *Wt*, 196.0 ± 10.34 and *Sarm1* KO, 183.3 ± 10.5 nerves (mean and SEM, $n = 4$; $p = 0.4857$). (M) The percentage of myelinated versus non-myelinated axons present in both *Wt*, 99.3 ± 0.09 and *Sarm1* KO, 99.41 ± 0.04 nerves is not different (mean and SEM, $n = 4$; $p = 0.3429$). (N) Myelin sheath thickness as depicted by g-ratios is similar in both *Wt*, 0.69 ± 0.007 and *Sarm1* KO, 0.704 ± 0.003 nerves (mean and SEM, $n = 4$; $p = 0.4857$). (O) Scatter plot of g-ratio as a function of axonal caliber in *Wt* sciatic nerves. (P) Scatter plot of g-ratio as a function of axonal caliber in *Sarm1* KO sciatic nerves.

(Figure 6A; Zhu et al., 2019; Uccellini et al., 2020). Additionally, we found no differences in protein levels for EGR2/KROX-20, JUN, and myelin proteins, myelin protein zero (MPZ) and MBP (Figures 6B-G).

Thus, myelination and myelin maintenance are unperturbed and myelin gene and protein expression are normal in the PNS in the absence of *Sarm1* in the mouse.

CNS myelination and myelin gene expression are normal in the *Sarm1* KO mouse

We have shown that oligodendrocytes in the dorsal and ventral spinal cord of *Sarm1* mutant zebrafish larvae myelinate normally. To confirm whether CNS myelination is also unaffected in *Sarm1* KO mice, we assessed adult P60 optic nerves by EM. We found that

Sarm1 KO optic nerves were morphologically indistinct from *Wt* samples, with similar numbers of total axons, ratio of myelinated to unmyelinated axons, g-ratio and a similar cross-sectional nerve area (Figures 7A-G and Supplementary Figure 5E). Furthermore, by qPCR, *Sarm1* KO optic nerves showed no differences in gene expression for oligodendrocyte/myelin markers (*Mbp*, *Olig2*, *Plp1*, *Sox10*), cytokine or chemokine expression (*Ccl2*, *Ccl3*, *Ccl4*, *Ccl5*, *IL1b*, *IL6*), apart from an upregulation of *IL10* (Figure 7H). Interestingly although there was a significant difference in *Sarm1* mRNA expression between *WT* and *KO* samples, as one would expect, we did not detect any upregulation of *Xaf1* in the optic nerve (Figure 7H). We also tested MBP protein levels by western blot in *Sarm1* KO optic nerves and found no differences compared to *WT* nerves (Figures 7I, J).

In conclusion there are no observable defects in myelin in adult *Sarm1* KO mouse optic nerves.

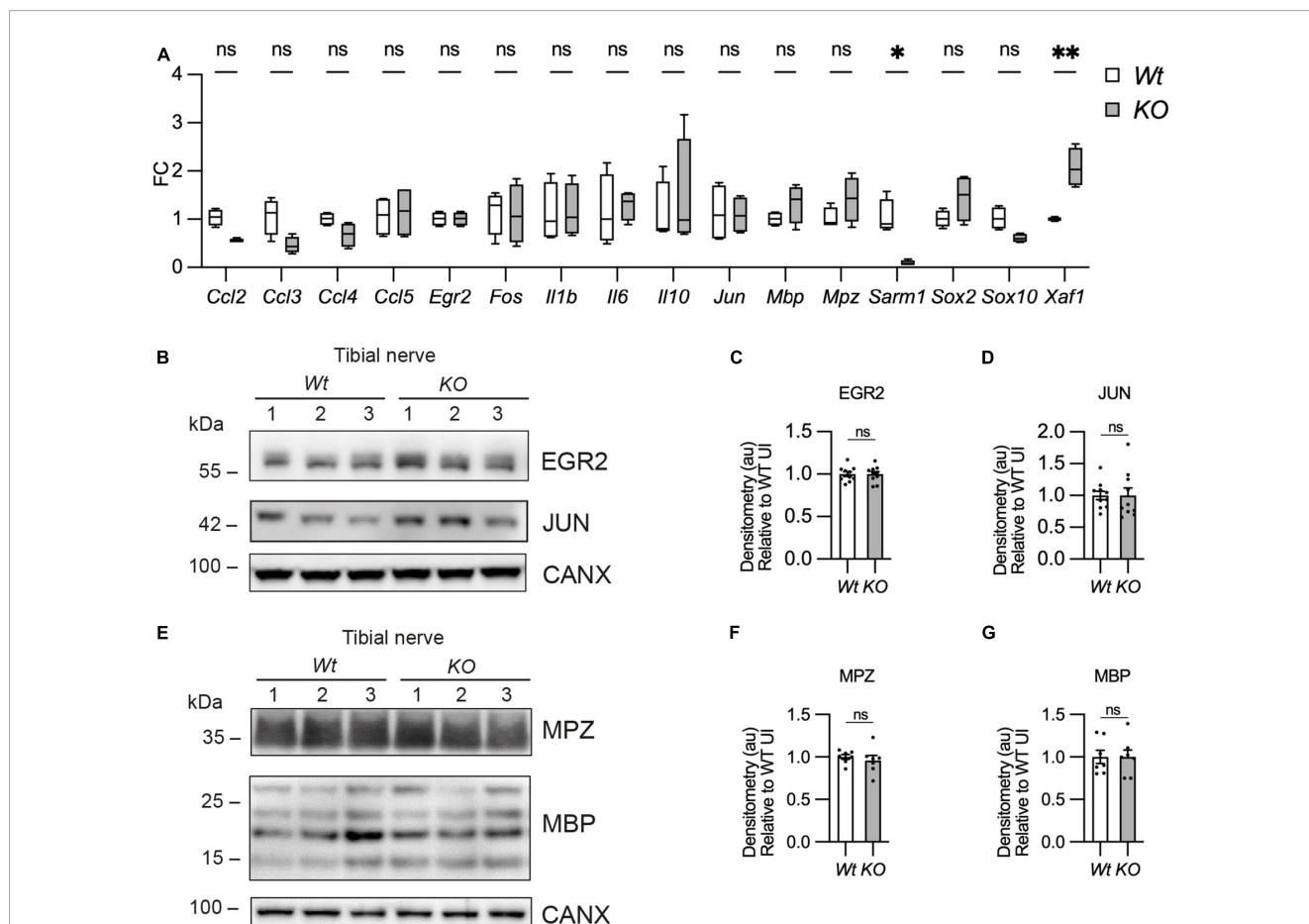


FIGURE 6 Myelin gene expression is normal in *Sarm1* null peripheral nerves. **(A)** Relative mRNA expression for chemokine, Schwann cell injury and myelin genes in the P60 uninjured tibial nerve of *Wt* and *Sarm1* KO mice. All fold change values normalized to uninjured *Wt* tibial nerve ($n = 4$; * $p < 0.05$, ** $p < 0.01$). **(B)** Representative Western blot image of tibial nerve protein extracts from P60 *Wt* and *Sarm1* KO mice. The image shows no difference in levels of EGR2 and JUN, between *Wt* and *Sarm1* KO nerves. **(C)** There is no significant difference in EGR2 levels in *Wt* and *Sarm1* KO nerves ($n = 7$; $p = 0.9118$). EGR2 protein levels are normalized to the levels in *Wt* nerves, which are set as 1. **(D)** There is no significant difference in JUN levels in *Wt* and *Sarm1* KO nerves ($n = 7$; $p = 0.5787$). The quantifications are normalized to the levels in *Wt* nerves, which are set as 1. **(E)** Representative Western blot image showing no difference in levels of Myelin protein zero (MPZ) and Myelin basic protein (MBP), between P60 *Wt* and *Sarm1* KO nerves. **(F)** There is no significant difference in MPZ levels in *Wt* and *Sarm1* KO nerves ($Wt n = 6$; $KO n = 5$; $p = 0.3176$). The quantifications are normalized to the levels in *Wt* nerves, which are set as 1. **(G)** There is no significant difference in MBP levels in *Wt* and *Sarm1* KO nerves ($n = 7$; $p > 0.9999$). The quantifications are normalized to the levels in *Wt* nerves, which are set as 1.

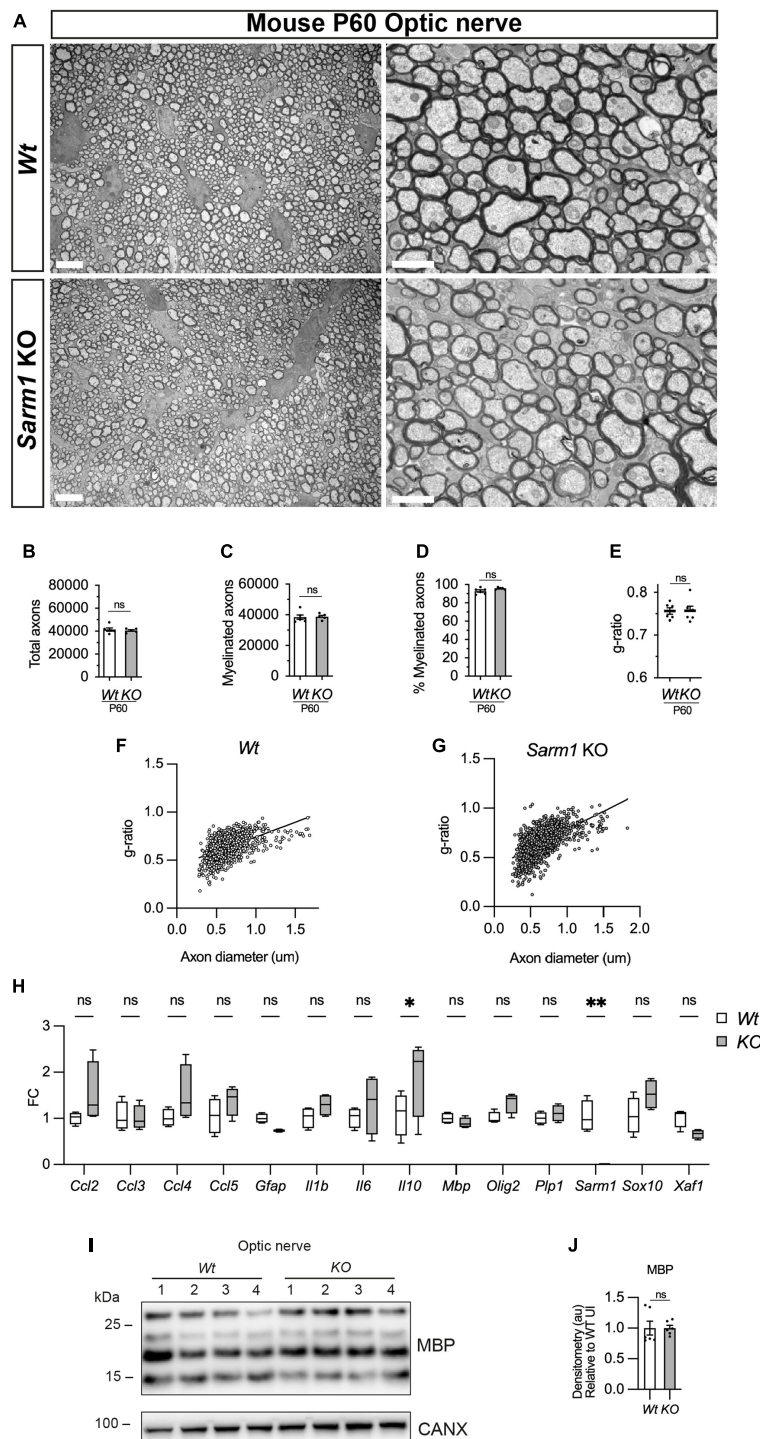


FIGURE 7

Optic nerve myelination is normal in *Sarm1* null mice. **(A)** Representative electron micrographs taken at x 3,000 (left hand side panels) and x 12,000 (right hand side panels) magnification from adult *Wt* and *Sarm1* KO optic nerves at postnatal day 60 (P60). There are no ultrastructural differences in the optic nerves of *Sarm1* KO compared to those of *Wt* animals. Scale bar 5 μm (x 3,000) and 2 μm (x 12,000). **(B)** The total number of axons quantified per optic nerve profile are not significantly different between *Wt*, 41422 ± 1375 and *Sarm1* KO, 40484 ± 786 (mean and SEM, $n = 6$ *Wt*; $n = 5$ KO; $p = 0.9307$). **(C)** The number of myelinated axons quantified in *Wt*, 38457 ± 1441 and *Sarm1* KO, 38782 ± 852.9 optic nerves is similar (mean and SEM, $n = 6$ *Wt*; $n = 5$ KO; $p = 0.4286$). **(D)** The percentage of myelinated axons quantified in *Wt*, 92.8 ± 1.2 and *Sarm1* KO, 95.9 ± 0.5 optic nerves is not significantly different (mean and SEM, $n = 6$ *Wt*; $n = 5$ KO; $p = 0.0736$). **(E)** Myelin sheath thickness as depicted by g-ratios is similar in both *Wt*, 0.757 ± 0.007 and *Sarm1* KO, 0.757 ± 0.01 optic nerves (mean and SEM, $n = 6$; $p = 0.9610$). **(F)** Scatter plot of g-ratio as a function of axonal caliber in *Wt* optic nerves. **(G)** Scatter plot of g-ratio as a function of axonal caliber in *Sarm1* KO optic nerves. **(H)** Relative mRNA expression for chemokine, oligodendrocyte and myelin genes in the P60 uninjured optic nerve of *Wt* and *Sarm1* KO mice. All fold change values normalized to uninjured *Wt* optic nerve ($n = 4$; * $p < 0.05$, ** $p < 0.01$). **(I)** Representative western blot image of optic nerve protein extracts shows no difference in levels of MBP, between *Wt* and *Sarm1* KO nerves. **(J)** There is no significant difference in MBP expression between *Wt* and *Sarm1* KO optic nerves ($n = 6$; $p = 0.3939$). The quantifications are normalized to the levels in uninjured *Wt* nerves, which are set as 1.

Discussion

A number of studies investigating the role of SARM1 in the nervous system have documented that PNS and CNS myelin appears normal in the adult *Sarm1* KO mouse however there have been no in-depth quantitative studies of both PNS and CNS myelination to confirm or refute this (Osterloh et al., 2012; Geisler et al., 2016; Marion et al., 2019; Ko et al., 2020). Additionally, there has been one study that generated a Crispr-Cas9 *sarm1* mutant zebrafish however they did not comment on whether PNS or CNS myelination was normal (Tian et al., 2020). Furthermore, there have been no studies investigating whether SARM1 is present in PNS and CNS myelinating glia.

SARM1, unlike other members of the MyD88 family, is abundant in the murine nervous system, particularly in neurons (Kim et al., 2007; Chen et al., 2011). SARM1 protein is not found in mouse microglia but is expressed in astrocytes and plays a role in neuroinflammation (Lin et al., 2014; Liu et al., 2021; Jin et al., 2022). We have shown that SARM1 is present in mouse oligodendrocytes *in vitro* and *in vivo* and zebrafish oligodendrocytes express *sarm1* mRNA. In contrast, Schwann cells and satellite glia do not contain detectable SARM1 protein and *sarm1/Sarm1* mRNA is found at very low levels in Schwann cells in developing zebrafish larvae and in mouse cell culture. Additionally, cultured mouse Schwann cells are insensitive to application of high dose specific SARM1 activators, whereas cultured oligodendrocytes undergo cell death. We have also shown that in the absence of Sarm1/SARM1, PNS and CNS myelination proceeds normally in both zebrafish and mice and that SARM1 does not play a role in myelin maintenance in the murine PNS or CNS. This adds to previous findings that conduction velocities measured by neurophysiological investigation of adult *Sarm1* KO mouse sciatic nerves were similar to control mice and that *Sarm1* KO adult mice have normal myelinated axon numbers in the corpus callosum (Geisler et al., 2016; Marion et al., 2019). Interestingly, a previous study found a small but statistically significant reduction in myelin sheath thickness in the corpus callosum that was present in young but not older *Sarm1* KO mice (Marion et al., 2019). We did not find any difference in developmental myelination in the spinal cord of mutant *sarm1* zebrafish and we found no difference in g-ratios between adult *Wt* and *Sarm1* KO mice in the optic nerve, confirming previous findings (Ko et al., 2020). However, it remains possible that *Sarm1* may have a role in developmental myelination in certain regions of the CNS.

In the PNS, in addition to Schwann cells, we have also shown that satellite glia, do not appear to have identifiable levels of SARM1 protein. SARM1 is also unlikely to be present at high levels in PNS resident macrophages since studies on other peripheral macrophage populations found relatively low levels of SARM1 in these cells and no effect of *Sarm1* deletion on macrophage function or gene expression (Kim et al., 2007; Uccellini et al., 2020).

It has been postulated that one of the purposes of SARM1, a toll like adapter protein and remnant of the innate immune system, and the wider axon degeneration machinery is to bring about compartmentalized neurodegeneration to prevent spread of viral pathogens throughout the nervous system (Tsunoda, 2008). In mouse CNS myelinating cocultures, loss of *Sarm1* protects neuronal somas against infection and cell death (Crawford

et al., 2022). Zika virus preferentially infects oligodendroglia and astroglia in neuron/glia cocultures and causes glia cell death (Cumberworth et al., 2017). Activation of SARM1 is known to cause neuronal cell body death independently of axonal degeneration and in this study we have shown that it can cause oligodendroglial death (Sasaki et al., 2020; Loreto et al., 2021). It is currently unknown if CNS glial cells upregulate *Sarm1* expression in response to zika infection and whether the glial cell death is SARM1 dependent? Additionally, oligodendrocyte death is curbed in the *Sarm1* KO mouse in a neuroinflammatory model of glaucoma. The authors postulate that the death is likely secondary to the role of Sarm1 in axons yet there remains the intriguing possibility that *Sarm1* may, in addition, be required cell-autonomously in oligodendrocytes for some or all of the cell death in this model (Ko et al., 2020). Interestingly, astrocytes do appear to upregulate expression of SARM1 in response to spinal cord injury and also to modulate neuroinflammation in experimental autoimmune encephalomyelitis (Liu et al., 2021; Jin et al., 2022). Finally, *Sarm1* KO mice demonstrate less myelin loss after traumatic brain injury, independent from protection against axon loss (Marion et al., 2019). Given that we have identified SARM1 in oligodendrocytes, it is possible that SARM1 may have a role in demyelination in the CNS.

In summary, we have shown, using the two commonest laboratory organisms for modeling neurological disease, that both *sarm1/Sarm1* mRNA and SARM1 protein are abundant in oligodendrocytes but not in Schwann cells. While SARM1 mutations have started to be identified as contributory to neurological diseases such as ALS (Gilley et al., 2021; Bloom et al., 2022), the question of whether SARM1 mutants are solely pathological in neurons or whether their expression in glia, such as astrocytes and oligodendrocytes, is contributory to the pathology, is now particularly pertinent. Even though we have investigated two commonly used vertebrate animal models in this study, it will be important in the future to investigate SARM1 expression and function in human PNS and CNS glia. However, our data remains consistent with the view that targeted knockdown or inhibition of SARM1 function is a promising strategy to ameliorate various neurological diseases, such as ALS or chemotherapy induced neuropathy, as this is unlikely to aberrantly affect PNS or CNS myelin in humans.

Materials and methods

Animals

All zebrafish research complied with the Animals (Scientific Procedures) Act 1986 and the University of Cambridge Animal Welfare and Ethical Review Body (AWERB), project license code P98A03BF9. Zebrafish (*Danio rerio*) were maintained at 28°C. *Tg[mbp:eGFPCAAX]* fish were a gift from Dave Lyons (Almeida et al., 2011), and *Sarm1*¹¹¹⁹³ mutant fish were obtained from ZIRC (Kettleborough et al., 2013). *Tg[mbp:eGFPCAAX]* and *sarm1*¹¹¹⁹³ embryos were obtained by natural spawning and raised in E3 medium (5 mM NaCl, 0.17 mM KCl, 0.33 mM CaCl₂, 0.3 mM MgSO₄, and 0.1% methylene blue) in Petri dishes

until 24 h post fertilization. Embryos were then incubated in E3 medium supplemented with 0.003% phenylthiourea (PTU) to prevent pigmentation. F2 generation fish were used for analysis. *sarm1*^{+/+} (*wt*) were compared to *sarm1*^{SA11193/SA11193} (*sarm1* mutant) for all experiments. Mouse research complied with European Union guidelines and protocols were approved by the Comité de Bioética y Bioseguridad del Instituto de Neurociencias de Alicante, Universidad Miguel Hernández de Elche and Consejo Superior de Investigaciones Científicas¹, Reference number 2017/VSC/PEA/00022 tipo 2. *Sarm1* knockout mice on C57BL/6J background (Kim et al., 2007) were bred from heterozygote crosses and F1 littermates were used for analysis. Mice were genotyped as previously described (Kim et al., 2007). *Tg[Plp1-cre/ERT2]* mice (MGI:2663093), expressing Cre recombinase under a tamoxifen inducible Proteolipid 1 (*Plp1*) promoter; *Tg[Sox10-cre]* mice (MGI:3586900), expressing Cre recombinase under control of the *Sox10* promoter; and *B6.Cg-Gt(ROSA)26Sor^{TM14}(CAG-tdTomato)Hze/J* (MGI:3813512) that express tdTomato upon removal of a floxed stop codon under control of the *Rosa26* locus were all obtained from Jackson Laboratories (Leone et al., 2003; Matsuoka et al., 2005; Madisen et al., 2010). *Tg[Plp1-cre/ERT2]* mice received an injection of 100 mg kg⁻¹ tamoxifen during 5 consecutive days at P45. Tamoxifen (Sigma-Aldrich) was dissolved in corn oil (Sigma-Aldrich) and absolute ethanol (Merck) (10:1). Nerves were fresh frozen after two weeks of first tamoxifen injection.

Genotyping zebrafish

Zebrafish genomic DNA was isolated from adult zebrafish fins and incubated at 55°C overnight with 0.5 mg mL⁻¹ Proteinase K in a 10 mM Tris-HCL buffer containing 50 mM KCL and 10% Tween20 and 10% NP40. PCR was run using primers, Forward: 5'-TCTGGAGCTGGTGGAGCCCT-3'; Reverse: 5'-AGTCTAGTTTCTGCCTGACCTTGG-3'. PCR product was then restriction enzyme digested at 37°C for 1 h with *MseI* (New England Biolabs) and then run on a 1.5% Agarose gel. WT PCR product produces a band of 233 base pairs. Mutant PCR product produces two bands of 165 and 68 base pairs.

Plasmids and microinjection

To generate the *neuroD:tdTomato* construct, the p-5E neurod5kb promoter entry vector (Mo and Nicolson, 2011), gifted by Dr. A. Nechiporuk, was inserted along with pME tdTomato (Oehlers et al., 2015), gifted by Dr D. Tobin (Addgene plasmid #135202) and p3EpolyA into pDestTol2pA2 using the GatewayTM system as previously described (Kwan et al., 2007). To visualize posterior lateral line neurons, 20 pg of the *neuroD:tdTomato* construct were microinjected into one cell stage embryos. Larvae were then fluorescently sorted at 4dpf.

¹ <http://in.umh-csic.es/>

2-photon axotomy of PLL axons in larval zebrafish

Axotomies were carried out at the Cambridge Advanced Imaging Centre on a TriM Scope II two-photon Scanning Fluorescence Microscope using Imspector Pro software (LaVision Biotec) and a near-infrared laser source (Insight DeepSee, Spectra-Physics). The laser light was focused by a 25x, 1.05 Numerical Aperture water immersion objective lens (XLPLN25XWMP2, Olympus). Axotomies were carried out by focusing the laser at a 6 × 6 μm section of the posterior lateral line using 100% laser power.

Schwann cell culture

Freshly plated mouse Schwann cells were obtained from sciatic and brachial nerves from postnatal day 2-4 mice (P2-4). Nerves were digested with trypsin and collagenase, centrifuged and plated on laminin/Poly-L-lysine (PLL) coated glass coverslips in defined medium as previously described (Arthur-Farraj et al., 2011).

Measurement of intracellular NAD⁺

Schwann cells were directly plated on PLL coated 24 well plates and maintained in DMEM/5% horse serum (HS). Schwann and HEK 293T cells were treated with 100 μM vacor, 250 μM 3-AP, or vehicle controls, and collected in media at 0 h and 72 h after treatment. Protein was extracted using PierceTM IP Lysis Buffer supplemented with cOmpleteTM Mini EDTA-free Protease Inhibitor Cocktail, and a Bicinchoninic acid (BCA) assay carried out to determine protein concentration. All samples were diluted to 0.5 μg μL⁻¹. The NAD-glo assay was performed according to manufacturer's instruction of the NAD⁺/NADH-GloTM assay by Promega (G9071). In short, 25 μL of sample were incubated with 12.5 μL 0.4 M HCl at 60°C for 15 min, before 12.5 μL 0.5 M Tris base were added. 10 μL NAD⁺ standards or sample were then mixed with 10 μL NAD-glo master mix (1 mL luciferin detection reagent, 5 μL reductase, 5 μL reductase substrate, 5 μL NAD⁺ cycling enzyme, 25 μL NAD⁺ cycling substrate) and incubated at RT for 40 min. Luminescence was read using a GloMax[®] Explorer microplate reader and NAD⁺ concentrations determined relative to a NAD⁺ standard curve.

Oligodendrocyte cell culture

Sprague-Dawley neonatal (≤ P7) rat pups were decapitated following lethal overdose with pentobarbital. The brains were dissected and submerged into Hibernate-A low fluorescence media (Transnetyx Tissue, #HALF). The tissue was cut into 1-mm³ pieces, washed in HBSS^{-/-} (Gibco, # 11039047), then spun down at 100 g for 1 min at room temperature. To digest the tissue, the tissue was incubated in 34 U mL⁻¹ papain (Worthington, #LS003127) and 40 μg mL⁻¹ DNase I (Sigma, #D5025) in HALF, and incubated on an orbital shaker (55 rpm) for 40 min at 37°C. To obtain a single-cell suspension, the tissue was triturated in HALF supplemented

with 2% B27 and 2 mM sodium pyruvate, first using a 5 mL serological pipette and then three fire-polished glass pipettes of descending diameter. The supernatant containing the cells was filtered through 70 μm strainers into a tube containing 90% isotonic Percoll (GE Healthcare, #17-0891-01, in $10 \times$ PBS pH 7.2 (Gibco, #70013032). The final volume was topped up with DMEM/F12 (Gibco, #31331028) then inverted several times to yield a homogenous suspension with a final Percoll concentration of 22.5%. The single cell suspension was then separated from tissue and myelin debris by gradient density centrifugation at 800 g (without brakes) for 20 min at room temperature. The myelin debris and supernatant were aspirated, leaving only the cell pellet, which was then resuspended in HBSS^{-/-} to wash out the Percoll. Subsequently, red blood cell lysis buffer (BD Biosciences, #555899) was used to remove red blood cells. OPCs were isolated by positive selection using 2.5 μg A2B5 (Merck Millipore, #MAB312) primary antibody, followed by 20 μL of rat anti-mouse IgM antibody (Miltenyi, #130-047-302) per brain using the MACS protocol according to the manufacturer's instructions. To collect the A2B5⁺ fraction, the MACS MS column (Miltenyi, #130-042-201) was removed from the magnetic stand (Miltenyi, #130-042-102) and cells were flushed from the column with 1 mL of prewarmed OPC medium (DMEM F/12 containing N-Acetyl cysteine (60 μg mL⁻¹, Sigma, #A9165), human recombinant insulin (10 μg mL⁻¹), sodium pyruvate (1 mM, Thermo Fisher, #11360-070), apo-transferrin (50 μg mL⁻¹, Sigma, #T2036), putrescine (16.1 μg mL⁻¹, Sigma, #P7505), sodium selenite (40 ng mL⁻¹, Sigma, #S5261), progesterone (60 ng mL⁻¹, Sigma, #P0130), bovine serum albumin (330 μg mL⁻¹, Sigma, #A4919). Cells were counted, then seeded at a density of 20,000 cells/cm² on poly-D-lysine (5 μg mL⁻¹ PDL, Sigma #P6407) coated plates.

Freshly isolated OPCs were cultured in OPC medium containing proliferation factors, b-FGF (30 ng mL⁻¹, Peprotech, #100-18B) and PDGF (30 ng mL⁻¹, Peprotech, #100-13a) then changed into OPC media containing T3 (Triiodothyronine, Sigma, #T2877) for 5-7 days to induce OPC to oligodendrocyte differentiation. Whilst in culture, cells were maintained in a humidified incubator at 37°C, 5% CO₂, 5% O₂, with media changes every 48 h.

Quantification of vacor treated oligodendrocyte cultures

Rat oligodendrocyte cultures were fixed at various time points following DMSO and Vacor treatment. These cells were immunofluorescently labeled with DAPI and an antibody to SOX10. Three representative images taken at 20x across cultures at different time points were quantified using Fiji for the presence of SOX10 expression. This experiment was repeated three times and average numbers of SOX10 positive oligodendrocytes counted per frame were represented.

In situ hybridization chain reaction (HCR)

Embryos were fixed using 4% paraformaldehyde in calcium and magnesium free phosphate buffered saline (PBS) and stored at -20°C in 100% MeOH. HCR 3.0 was performed as described in

(Choi et al., 2018). In short, 2 pmol HCR probes were hybridized at 37°C overnight in hybridization buffer, followed by repeated washing in wash buffer. Probes were detected using 30 pmol fluorescent hairpins in amplification buffer overnight at room temperature followed by washing in $5 \times$ SSC 0.001% Tween-20. Samples were finally counterstained using 1 μg mL⁻¹ DAPI and mounted in 80% glycerol in a MatTek glass bottom dish. DNA probes for zebrafish *mbp*, *sarm1*, *sox10*, fluorescent hairpins and buffers were purchased from Molecular Instruments, Inc.

Imaging and image analysis

Mouse optic nerves were imaged on a Zeiss LSM 900 with airyscan 2, 63x oil objective. Fish were imaged on a Zeiss LSM 700 confocal microscope with a 40x oil objective or a Zeiss LSM 900 confocal microscope with a 63x oil objective. For imaging of living larvae, 4 or 5 days post-fertilization animals were anaesthetized in 0.01% tricaine (w/v) and embedded in 1% low melting point agarose (w/v in E3 media supplemented with 0.003% of PTU). For imaging of *Tg[mbp:eGFPCAAX]* zebrafish, images of the spinal cord and PLLn were obtained at the level of the first, third and seventh motor nerves distal to the urogenital opening. For live imaging after PLLn injury, images were taken every 10 min for up to 26 h and embryos maintained at 28°C. Survival of fish was monitored by observing heartbeat and circulation. Confocal images are displayed as grid-stitched maximum intensity projections produced using Fiji (Preibisch et al., 2009; Schindelin et al., 2012). For fluorescence intensity measurements of *Tg[mbp:eGFPCAAX]* fish, integrated densities were obtained from regions of interest. For *mbp* HCR quantification, images of the PLLn and spinal cord were obtained at the level of the first, third and seventh motor nerves distal to the urogenital opening. For statistics coding of color by the intensity of the *mbp* signal, nuclear segmentation was conducted in Imaris (Bitplane) using a surface mask around the DAPI stain with a surface detail of 0.22 μm , and touching surfaces were split using a seed size of 4 μm . For signal intensity analysis, surfaces for the spinal cord and posterior lateral line were drawn in Imaris (Bitplane) and intensity sum of both *mbp* and DAPI signals determined. Intensity was then normalized by the area of the surface. For all experiments between seven to nine fish were imaged (spinal cord and one PLLn) per genotype.

Antibodies

Immunofluorescence: SOX10 (R&D Systems, 1:100, AF2864, [RRID:AB_442208](#)) donkey anti-goat IgG (H + L) Alexa Fluor 488 (Invitrogen, 1:1000, A11057), Anti-Beta III Tubulin (Sigma Aldrich, 1:1000, AB9354, [RRID:AB_570918](#)), NF200 (Abcam, 1:1000, ab72997, [RRID:AB_1267598](#)), SARM1 rabbit polyclonal antibodies (kind gift from Professor Hsueh, 1:500) and purchased from Abcam (Ab226930, 1:2000, [RRID:AB_2893433](#)), tdTomato (SIGGEN, 1:500, [RRID:AB_2722750](#)) donkey anti-goat IgG (H + L) Alexa Fluor 488 (Invitrogen, 1:1000, A11057), Cy3 donkey anti-rabbit IgG (H + L) (Jackson ImmunoResearch, 1:500, 711-165-152), Donkey anti-Mouse IgG (H + L) Highly Cross-Adsorbed Seco Alexa Fluor 488 (Invitrogen, 1:1000, A-21202), Donkey anti-Chicken IgY, Alexa Fluor 647 (Merck, 1:1000, 15389818), DAPI (Thermo scientific, 1:2000, 62248).

Western blot: CALNEXIN (Enzo Life Sciences, 1:1000, ADI-SPA-860-D, [RRID:AB_312058](#)), JUN (Cell Signalling Technology, 1:1000, 9165, [RRID:AB_2130165](#)), EGR2 (EMD Millipore, 1:500, ABE1374, [RRID:AB_2715555](#)), MPZ (Aves Labs, 1:2000, PZO, [RRID:AB_2313561](#)), MBP (EMD Millipore, 1:1000, AB9348, [RRID:AB_2140366](#)), Anti-mouse IgG HRP-linked antibody (Cell Signaling Technology, 1:2000, 7076S), Anti-rabbit HRP-linked antibody (Cell Signaling Technology, 1:2000, 7074S), Goat pAb to Chicken IgY H + L (HRP) (Abcam, 1:2000, ab97135).

Immunofluorescence

Sciatic and optic nerves were dissected from *Wt* and *Sarm1* KO mice and directly embedded in O.C.T. compound, without fixing, and stored at -80°C until ready for cryosectioning. Cryosections at $5\ \mu\text{m}$ thick were collected onto SuperFrost plus slides. These slides were post-fixed in 4% PFA at room temperature for 10 min followed by three washes of 5 min each with 1xPBS. The slides were then immersed in 100% methanol at -20°C for 10 min, followed by three washes of 5 min each with 1xPBS. For anti-Tdtomato sections were immersed in 100% Acetone for 5 min at room temperature before blocking solution was added. The slides were then blocked in 5% horse serum (HS)/0.2% Triton x-100/PBS for 30 min at room temperature. Primary antibodies were diluted in blocking solution and slides were incubated overnight at 4°C . The following day, the slides were washed once for 5 min with 1xPBS, twice for 5 min with 0.1% tween/PBS and finally once again for 5 min with 1xPBS before adding secondary antibodies. The corresponding secondary antibodies were diluted at 1:500 along with DAPI at 1:2,000 for 2 h at room temperature and kept in the dark. Slides were then washed once for 5 min with 1xPBS, twice for 5 min with 0.1% tween/PBS and finally once again for 5 min with 1xPBS before mounting using Fluorsave (Calbiochem, 345789) and representative images were taken using Leica DMI6000B at 40x, 63x, and 100x. The same protocol was followed for immunofluorescence staining in rat oligodendrocyte cultures and representative images were taken at 20x using Leica DMI8.

Western blot

Homogenates were obtained from sciatic or optic nerves. These lysates were prepared as described previously ([Gomez-Sanchez et al., 2015](#)). Samples were homogenized in ice-cold RIPA buffer with HaltTM Protease Inhibitor Cocktail (100X) (ThermoFisher Scientific 78429). After homogenization, the samples were incubated on ice for 30 min for further lysis. The resulting lysate was centrifuged at 12,000 rpm. at 4°C , and the supernatant was taken for the Bicinchoninic acid (BCA) assay (ThermoFisher, 23227). The supernatant was diluted in loading buffer and boiled at 95°C for 5 min. For western blot analysis of SARM1, 20 μg of protein was loaded, for JUN and EGR2, 15 μg of protein was loaded and for analysis of myelin proteins MPZ and MBP, 7.5 μg of protein was loaded. Next, the samples were run in SDS-PAGE and transferred onto a PVDF membrane. After blocking the membrane in 5% skimmed milk (diluted in TBS/0.1% Tween) for 1 h,

the membrane was incubated overnight at 4°C with primary antibodies listed. Experiments were repeated at least three times with fresh samples and representative photographs are shown. Densitometric quantification was done using ImageJ. Measurements were normalized to the loading control Calnexin or Beta Actin.

RNA extraction and qPCR

RNA was extracted from P60 tibial or optic nerves using Trizol (Invitrogen, 15596026) as previously described ([Arthur-Farraj et al., 2017](#)). Nerves from two mice were pooled together for each biological replicate. The integrity and quantity of RNA was determined using Nanodrop (ThermoFisher Scientific) and Agilent 2100 Bioanalyzers (Agilent Technologies). 500 ng of RNA was used per biological replicate for cDNA conversion using QuantiTect reverse transcription kit (Qiagen, 205311). qPCR was run on a BioRad CFX96 using iTaq with SYBR Green (BioRad, 1725124). *Ankrd27* and *Canx* were used as housekeeping genes. Two technical replicates and five biological replicates were run per experiment. Fold change was calculated using the delta CT method. All primers were designed using Primer blast (NCBI) ([Ye et al., 2012](#)).

Primer sequences

Gene name	Forward Primer sequence	Reverse Primer sequence
<i>Ankrd27</i>	TCTGCCAGTTCGAGTCCTAT	AATGACGACAGCCTTCCATC
<i>Canx</i>	CTTCCAGGGATAAAGGACTTGT	ACATAGGCACCACCATTCTA
<i>Ccl2</i>	AGGCTGGAGAGTACAAGAGG	CCCATTCCTTCTGGGGTCAG
<i>Ccl3</i>	TGCCCTTGCTGTTCTCTCT	GTGGAATCTTCCGGCTGTAG
<i>Ccl4</i>	AAGCTGCCGGGAGGTGTAAG	TGCTGCCCTCTCTCTCTCTGT
<i>Ccl5</i>	TGCCACGTC AAGGAGTATTTT	TCCTAGCTCATCTCCAATAGTTGATG
<i>Egr2</i>	CCGTATCCGAGTAGCTTCGC	TCAATGGAGAATTTGCCCATGT
<i>Gfap</i>	GGGCGAAGAAAACCGCATCA	TCACCATCCCGCATCTCCA
<i>Fos</i>	GGTTTCAACGCCGACTACGA	GTTGGCACTAGAGACGGACAG
<i>Il1b</i>	GCCACCTTTTGACAGTGATGAGA	ATCAGGACAGCCAGGTCAA
<i>Il6</i>	GCCTTCTTGGGACTGATGCT	GCCATTGCACAACCTTTTCTCA
<i>Il10</i>	GAGAAGCATGGCCAGAAATCAA	AAAATCACTCTTCACTGCTCCA
<i>Jun</i>	CCTTCTACGACGATGCCCTC	GGTTC AAGGTCATGCTCTGTTT
<i>Mbp</i>	AATCGGCTCACAAGGATTC A	TCCTCCAGCTTAAAGATTTTGG
<i>Mpz</i>	CGGACAGGGAATCTATGGTGC	TGGTAGCGCCAGGTA AAGAG
<i>Olig2</i>	AACCCCGAAAGGTGTGGATG	TGGCCCAAGGATGATCTAA
<i>Plp1</i>	CCGCAAAACAGACTAGCCAAC	CAAGCCCATGTCTTTGGCAC
<i>Sarm1</i>	GGACCATGACTGCAAGGACTG	CCGTTGAAGGTGAGTACAGCC
<i>Sox2</i>	TCGAGGGAGTTTCGCAAAAG	ACCCAGCAAGAACCCTTTCC
<i>Sox10</i>	CTGCTATTCAGGCTCACTACAAGAG	CTCTGTCTTTGGGGTGGTTGG
<i>Xaf1</i>	GCTGATCTTCCACAGGAGAC	GAGTAAACCTCTGGCACTTCTC

Electron microscopy

Sciatic and optic nerves were processed as described previously ([Gomez-Sanchez et al., 2015](#)). Briefly, samples were fixed in 2.5% glutaraldehyde/2% paraformaldehyde in 0.1 M cacodylate buffer,

pH 7.4, overnight at 4°C. Samples were post-fixed with 1% OsO₄, embedded in Agar 100 epoxy resin. Transverse ultrathin sections from neonatal (P2) and adult (P60) sciatic nerves (5 mm from the notch) or from adult (P60) optic nerves (2 mm from the chiasm) were taken and mounted on film.

Photographs were taken using a Jeol 1010 electron microscope with a Gatan camera and software. Images were analyzed using ImageJ. Photographs of sciatic nerves were taken at 3,000 × magnification to measure the number of myelinated axons, non-myelinated axons bigger than 1.5 μm, and Schwann cell nuclei. The nerve area was measured from photographs taken at 200 × magnification. Photographs of optic nerves were taken at 12000x magnification to measure the number of myelinated and non-myelinated axons. The nerve area was measured from photographs taken at 200x magnification. G-ratios were calculated using AimSeg, a bioimage analysis workflow that combines machine learning, automated post-processing, and human instruction to conduct axon, inner cytoplasmic tongue, and compact myelin segmentation on electron microscope data (Rondelli et al., 2023). *N* = 4-6 for all experiments (4-6 biological replicates: 1 nerve per animal, 4-6 animals, 15-20 sections per nerve).

Statistical analysis

Statistical analyses were performed using Graph-Pad Prism software (version 9.1.2). Results are expressed as mean ± SEM. Statistical significance was estimated by Mann-Whitney U-test or unpaired, two tailed students t-test with Bonferonni correction for multiple testing where necessary. *P* < 0.05 was considered statistically significant. *N* numbers for all experiments are listed in the figure legends. All quantification was blinded to the assessor.

Data availability statement

The original contributions presented in this study are included in the article/[Supplementary material](#), further inquiries can be directed to the corresponding author.

Ethics statement

This animal study was reviewed and approved by University of Cambridge Animal Welfare and Ethical Review Body.

Author contributions

PA-F: conceptualization, writing – original draft, supervision, and project administration. PA-F, SE, CM, CC, AI-G, AL, and JG-S: methodology. SE, CM, CC, AC-B, AI-G, JG-S, and PA-F: investigation. MT, C-YC, Y-PH, RF, RB, KM, BS, MC, JG-S, and PA-F: resources. PA-F, SE, CM, CC, AL, JG-S, RB, and KM: writing – review and editing. PA-F, SE, and CM:

visualization. MC and PA-F: funding acquisition. All authors read and approved the manuscript.

Funding

CM was funded by a Medical Research Council (UK) studentship (2251399). PA-F (206634/Z/17/Z), AL (210904/Z/18/Z), CC (220027/Z/19/Z), RB (203151/Z/16/Z) and MC (220906/Z/20/Z) were funded by the Wellcome Trust (UK). BS was supported by a Henry Dale Fellowship jointly funded by the Wellcome Trust and the Royal Society (109408/Z/15/Z). KM was funded by the National Institute of Neurological Disorders and Stroke Awards (R01NS079445). JG-S was funded by a Miguel Servet Fellowship (CP22/00078) from the Instituto de Salud Carlos III and the Millennium Nucleus for the Study of Pain (MiNuSpain), Santiago, Chile. HC was funded by the Spanish “Ministerio de Economía y Competitividad” (BFU2016-75864R and PID2019-109762RB-I00), ISABIAL (UGP18-257 and UGP-2019-128), and Generalitat Valenciana (PROMETEO 2018/114). Y-PH and C-YC were funded by Academia Sinica, AS-IA-106-L04 to Y-PH. For the purpose of Open Access, the author has applied a CC BY public copyright licence to any Author Accepted Manuscript version arising from this submission.

Acknowledgments

We thank David Lyons for the *Tg[MBP:eGFP/CAAX]* zebrafish. We thank members of the MC, BS, and KM labs for useful discussions. We thank Jiakun Chen for assistance with *Sarm1* mutant zebrafish and Kevin O’Holleran and the team at the Cambridge Centre for Advance Imaging for assistance with microscopy. We thank Drs. Stefanie Kaech Petrie and Crystal Chaw of the Jungers Centre for Neurosciences Research for help with setting up laser axotomy in larval zebrafish. We thank the EM platform at ISABIAL. We also thank Guillermina López-Bendito, Isabel Pérez-Otaño, and Ueli Suter for transgenic mouse lines.

Conflict of interest

MC was a consultant for Nura Bio.

The remaining authors declare that the research was conducted in the absence of any commercial or financial relationships that could be construed as a potential conflict of interest.

Publisher’s note

All claims expressed in this article are solely those of the authors and do not necessarily represent those of their affiliated organizations, or those of the publisher, the editors and the reviewers. Any product that may be evaluated in this article, or claim that may be made by its manufacturer, is not guaranteed or endorsed by the publisher.

Supplementary material

The Supplementary Material for this article can be found online at: <https://www.frontiersin.org/articles/10.3389/fncel.2023.1158388/full#supplementary-material>

SUPPLEMENTARY FIGURE 1

No first layer SARM1 antibody controls. **(A)** Representative immunofluorescence images of transverse sections of *Wt* and *Sarm1* KO mouse dorsal root ganglia (DRGs) to show lack of SARM1 (blue) signal in the absence of addition of primary antibody. NF-200 (neurofilament light chain; magenta) to show neurons. Scale bar 25 μm . **(B)** Representative immunofluorescence images of transverse sections of *Wt* and *Sarm1* KO mouse dorsal root ganglia (DRGs) to show lack of SARM1 (blue) signal in the KO sample in the presence the primary antibody. The *Wt* panel shows co-localization of NF-200 (magenta) positive neurons with SARM1 (blue). Scale bar 25 μm .

SUPPLEMENTARY FIGURE 2

sarm1 HCR no first layer controls. **(A)** MAX projection, lateral view of the PLLn of a 5dpf larva with no probes (no first layer control) to *sox10* nor *sarm1* applied. Images show DAPI (gray), and hairpins tagged to Alexa647 (magenta) and Alexa546 (green). Scale bar 25 μm . **(B)** MAX projection, lateral view of the spinal cord of a 5dpf larva with no antisense probes to *sox10* nor *sarm1* applied. Images show DAPI (gray), and hairpins tagged to Alexa647 (magenta) and Alexa546 (green). Scale bar 25 μm .

SUPPLEMENTARY FIGURE 3

Sarm1 mRNA but not SARM1 protein is detectable in mouse Schwann cells. **(A)** qPCR analysis of *Sarm1* expression in cultured mouse *Wt* and *Sarm1* KO DRGs and *Wt* and *Sarm1* KO Schwann cells [SC, $n = 4$ (4 biological replicates: 4 sciatic nerves from 2 animals pooled per biological replicate); ** $p < 0.01$]. **(B)** Freshly plated *Wt* and *Sarm1* KO, P2 dissociated mouse

Schwann cells both have undetectable levels of SARM1 protein (green). Cultures labelled for DAPI (gray) and SOX10 (magenta) ($n = 3$: two-four mice each from 3 L producing three separate cultures). Scale bar 50 μm .

SUPPLEMENTARY FIGURE 4

Cultured Schwann cells are insensitive to 3-AP induced cell death. **(A)** Dissociated and freshly plated P2 mouse Schwann cells cultured in defined medium with water or 250 mM 3-AP for 72 h show no cell death, judged by propidium iodide (PI) and DAPI nuclear staining and SOX10 immunocytochemistry, $101.6 \pm 1.7\%$ SOX10 positive cells survived after 72 h 250 mM 3-AP treatment (mean and SEM, $n = 3$: two-four mice, each from 3 L producing three separate cultures, $p = 0.68$). Scale bar 25 μm . **(B)** Intracellular NAD^+ levels decrease in HEK293 cells when treated for 72 h with 100 mM vacor. **(C)** Cultured rat oligodendrocytes (SOX10 positive; magenta) express SARM1 protein (green) using a commercial polyclonal anti-SARM1 antibody. Zoomed in area (indicated by dashed box). Arrowheads indicate SOX10 positive SARM1 positive cells. Scale bars 50 μm .

SUPPLEMENTARY FIGURE 5

Axon degeneration after PLLn laser abotomy is substantially delayed in absence of functional *Sarm1* in zebrafish larvae. **(A)** Schematic of overview of 2-photon laser abotomy of the PLLn (green) in larval zebrafish. **(B)** *wt* and *sarm1*^{SA11193/SA11193} (*sarm1* mutant) fish were injected at the one cell zygote stage with *neuroD:tdtomato* DNA constructs and 2-photon laser abotomy was performed in both genotypes at 4dpf. While *wt* PLLn axons start to degenerate around 3 h and are completely degenerated at 6 h post abotomy, PLLn axons in *sarm1* mutant larvae remain intact at least up until 26 h post imaging (imaging stopped due to UK home office regulations) ($n = 5$). Scale bar 100 μm . **(C)** The mean total nerve area of P2 mouse sciatic nerves in *Wt*, $27,674 \pm 2,050 \mu\text{m}^2$ and *Sarm1* KO, $33,527 \pm 2,648 \mu\text{m}^2$, is not significantly different (mean and SEM, $n = 5$; $p = 0.1508$). **(D)** Per nerve profile, the total nerve area of both *Wt* ($148,879 \pm 4,209 \mu\text{m}^2$) and *Sarm1* KO ($147,181 \pm 3,619 \mu\text{m}^2$) nerves is very similar ($n = 4$; $p = 0.8857$). **(E)** Per nerve profile, the total nerve area of both *Wt* ($51,002 \pm 1,238 \mu\text{m}^2$) and *Sarm1* KO ($54,130 \pm 982.6 \mu\text{m}^2$) optic nerves were not significantly different (mean and SEM, $n = 6$ WT; $n = 5$ KO; $p = 0.1255$).

References

- Almeida, R. G., Czopka, T., Ffrench-Constant, C., and Lyons, D. A. (2011). Individual axons regulate the myelinating potential of single oligodendrocytes in vivo. *Dev. Camb. Engl.* 138, 4443–4450. doi: 10.1242/dev.071001
- Arthur-Farraj, P., and Coleman, M. P. (2021). Lessons from injury: How nerve injury studies reveal basic biological mechanisms and therapeutic opportunities for peripheral nerve diseases. *Neurotherapeutics* 18, 2200–2221. doi: 10.1007/s13311-021-01125-3
- Arthur-Farraj, P., Wanek, K., Hantke, J., Davis, C. M., Jayakar, A., Parkinson, D. B., et al. (2011). Mouse schwann cells need both NRG1 and cyclic AMP to myelinate. *Glia* 59, 720–733. doi: 10.1002/glia.21144
- Arthur-Farraj, P. J., Morgan, C. C., Adamowicz, M., Gomez-Sanchez, J. A., Fazal, S. V., Beucher, A., et al. (2017). Changes in the coding and non-coding transcriptome and DNA methylome that define the schwann cell repair phenotype after nerve injury. *Cell Rep.* 20, 2719–2734. doi: 10.1016/j.celrep.2017.08.064
- Bloom, A. J., Mao, X., Strickland, A., Sasaki, Y., Milbrandt, J., and DiAntonio, A. (2022). Constitutively active SARM1 variants that induce neuropathy are enriched in ALS patients. *Mol. Neurodegener.* 17:1. doi: 10.1186/s13024-021-00511-x
- Bosanac, T., Hughes, R. O., Engber, T., Devraj, R., Brearley, A., Danker, K., et al. (2021). Pharmacological SARM1 inhibition protects axon structure and function in paclitaxel-induced peripheral neuropathy. *Brain* 144, 3226–3238. doi: 10.1093/brain/awab184
- Chen, C.-Y., Lin, C.-W., Chang, C.-Y., Jiang, S.-T., and Hsueh, Y.-P. (2011). Sarm1, a negative regulator of innate immunity, interacts with syndecan-2 and regulates neuronal morphology. *J. Cell Biol.* 193, 769–784. doi: 10.1083/jcb.201008050
- Chen, Y.-H., Sasaki, Y., DiAntonio, A., and Milbrandt, J. (2021). SARM1 is required in human derived sensory neurons for injury-induced and neurotoxic axon degeneration. *Exp. Neurol.* 339:113636. doi: 10.1016/j.expneurol.2021.113636
- Cheng, Y., Liu, J., Luan, Y., Liu, Z., Lai, H., Zhong, W., et al. (2019). Sarm1 gene deficiency attenuates diabetic peripheral neuropathy in mice. *Diabetes* 68, 2120–2130. doi: 10.2337/db18-1233
- Choi, H. M. T., Schwarzkopf, M., Fornace, M. E., Acharya, A., Artavanis, G., Stegmaier, J., et al. (2018). Third-generation in situ hybridization chain reaction: Multiplexed, quantitative, sensitive, versatile, robust. *Dev. Camb. Engl.* 145:dev165753. doi: 10.1242/dev.165753
- Coleman, M. P., and Höke, A. (2020). Programmed axon degeneration: From mouse to mechanism to medicine. *Nat. Rev. Neurosci.* 21, 183–196. doi: 10.1038/s41583-020-0269-3
- Crawford, C. L., Antoniou, C., Komarek, L., Schultz, V., Donald, C. L., Montague, P., et al. (2022). SARM1 depletion slows axon degeneration in a CNS model of neurotropic viral infection. *Front. Mol. Neurosci.* 15:860410. doi: 10.3389/fnmol.2022.860410
- Cumberworth, S. L., Barrie, J. A., Cunningham, M. E., de Figueiredo, D. P. G., Schultz, V., Wilder-Smith, A. J., et al. (2017). Zika virus tropism and interactions in myelinating neural cell cultures: CNS cells and myelin are preferentially affected. *Acta Neuropathol. Commun.* 5:50. doi: 10.1186/s40478-017-0450-8
- D’Rozario, M., Monk, K. R., and Petersen, S. C. (2017). Analysis of myelinated axon formation in zebrafish. *Methods Cell Biol.* 138, 383–414. doi: 10.1016/bs.mcb.2016.08.001
- Fogh, I., Ratti, A., Gellera, C., Lin, K., Tiloca, C., Moskvina, V., et al. (2014). A genome-wide association meta-analysis identifies a novel locus at 17q11.2 associated with sporadic amyotrophic lateral sclerosis. *Hum. Mol. Genet.* 23, 2220–2231. doi: 10.1093/hmg/ddt587
- Geisler, S., Doan, R. A., Cheng, G. C., Cetinkaya-Fisgin, A., Huang, S. X., Höke, A., et al. (2019a). Vincristine and bortezomib use distinct upstream mechanisms to activate a common SARM1-dependent axon degeneration program. *JCI Insight* 4:e129920. doi: 10.1172/jci.insight.129920
- Geisler, S., Huang, S. X., Strickland, A., Doan, R. A., Summers, D. W., Mao, X., et al. (2019b). Gene therapy targeting SARM1 blocks pathological axon degeneration in mice. *J. Exp. Med.* 216, 294–303. doi: 10.1084/jem.20181040
- Geisler, S., Doan, R. A., Strickland, A., Huang, X., Milbrandt, J., and DiAntonio, A. (2016). Prevention of vincristine-induced peripheral neuropathy by genetic deletion of SARM1 in mice. *Brain J. Neurol.* 139, 3092–3108. doi: 10.1093/brain/aww251
- Gerdtts, J., Summers, D. W., Sasaki, Y., DiAntonio, A., and Milbrandt, J. (2013). Sarm1-mediated axon degeneration requires both SAM and TIR interactions. *J. Neurosci.* 33, 13569–13580. doi: 10.1523/JNEUROSCI.1197-13.2013

- Gilley, J., and Coleman, M. P. (2010). Endogenous Nmnat2 is an essential survival factor for maintenance of healthy axons. *PLoS Biol.* 8:e1000300. doi: 10.1371/journal.pbio.1000300
- Gilley, J., Jackson, O., Pipis, M., Estiar, M. A., Al-Chalabi, A., Danzi, M. C., et al. (2021). Enrichment of SARM1 alleles encoding variants with constitutively hyperactive NADase in patients with ALS and other motor nerve disorders. *eLife* 10:e70905. doi: 10.7554/eLife.70905
- Gomez-Sanchez, J. A., Carty, L., Iruarrizaga-Lejarreta, M., Palomo-Irigoyen, M., Varela-Rey, M., Griffith, M., et al. (2015). Schwann cell autophagy, myelinophagy, initiates myelin clearance from injured nerves. *J. Cell Biol.* 210, 153–168. doi: 10.1083/jcb.201503019
- Gould, S. A., Gilley, J., Ling, K., Jafar-Nejad, P., Rigo, F., and Coleman, M. (2021a). Sarm1 haploinsufficiency or low expression levels after antisense oligonucleotides delay programmed axon degeneration. *Cell Rep.* 37:110108. doi: 10.1016/j.celrep.2021.110108
- Gould, S. A., White, M., Wilbrey, A. L., Pór, E., Coleman, M. P., and Adalbert, R. (2021b). Protection against oxaliplatin-induced mechanical and thermal hypersensitivity in Sarm1^{-/-} mice. *Exp. Neurol.* 338:113607. doi: 10.1016/j.expneurol.2021.113607
- Henninger, N., Bouley, J., Sikoglu, E. M., An, J., Moore, C. M., King, J. A., et al. (2016). Attenuated traumatic axonal injury and improved functional outcome after traumatic brain injury in mice lacking Sarm1. *Brain* 139, 1094–1105. doi: 10.1093/brain/aww001
- Huppke, P., Wegener, E., Gilley, J., Angeletti, C., Kurth, I., Drenth, J. P. H., et al. (2019). Homozygous NMNAT2 mutation in sisters with polyneuropathy and erythromelalgia. *Exp. Neurol.* 320:112958. doi: 10.1016/j.expneurol.2019.112958
- Jessen, K. R., and Mirsky, R. (2005). The origin and development of glial cells in peripheral nerves. *Nat. Rev. Neurosci.* 6, 671–682. doi: 10.1038/nrn1746
- Jin, L., Zhang, J., Hua, X., Xu, X., Li, J., Wang, J., et al. (2022). Astrocytic SARM1 promotes neuroinflammation and axonal demyelination in experimental autoimmune encephalomyelitis through inhibiting GDNF signaling. *Cell Death Dis.* 13:759. doi: 10.1038/s41419-022-05202-z
- Kettleborough, R. N. W., Busch-Nentwich, E. M., Harvey, S. A., Dooley, C. M., de Bruijn, E., van Eeden, F., et al. (2013). A systematic genome-wide analysis of zebrafish protein-coding gene function. *Nature* 496, 494–497. doi: 10.1038/nature11992
- Kim, Y., Zhou, P., Qian, L., Chuang, J.-Z., Lee, J., Li, C., et al. (2007). MyD88-5 links mitochondria, microtubules, and JNK3 in neurons and regulates neuronal survival. *J. Exp. Med.* 204, 2063–2074. doi: 10.1084/jem.20070868
- Ko, K. W., Milbrandt, J., and DiAntonio, A. (2020). SARM1 acts downstream of neuroinflammatory and necrotic signaling to induce axon degeneration. *J. Cell Biol.* 219:e201912047. doi: 10.1083/jcb.201912047
- Krauss, R., Bosanac, T., Devraj, R., Engber, T., and Hughes, R. O. (2020). Axons matter: The promise of treating neurodegenerative disorders by targeting SARM1-mediated axonal degeneration. *Trends Pharmacol. Sci.* 41, 281–293. doi: 10.1016/j.tips.2020.01.006
- Kwan, K. M., Fujimoto, E., Grabher, C., Mangum, B. D., Hardy, M. E., Campbell, D. S., et al. (2007). The Tol2kit: A multisite gateway-based construction kit for Tol2 transposon transgenesis constructs. *Dev. Dyn.* 236, 3088–3099. doi: 10.1002/dvdy.21343
- Leone, D. P., Genoud, S., Atanasoski, S., Grausenburger, R., Berger, P., Metzger, D., et al. (2003). Tamoxifen-inducible glia-specific Cre mice for somatic mutagenesis in oligodendrocytes and Schwann cells. *Mol. Cell. Neurosci.* 22, 430–440. doi: 10.1016/s1044-7431(03)00029-0
- LeWitt, P. A. (1980). The neurotoxicity of the rat poison vacor. A clinical study of 12 cases. *N. Engl. J. Med.* 302, 73–77. doi: 10.1056/NEJM19801103020202
- Lin, C.-W., Liu, H.-Y., Chen, C.-Y., and Hsueh, Y.-P. (2014). Neuronally-expressed Sarm1 regulates expression of inflammatory and antiviral cytokines in brains. *Innate Immun.* 20, 161–172. doi: 10.1177/1753425913485877
- Liu, H., Zhang, J., Xu, X., Lu, S., Yang, D., Xie, C., et al. (2021). SARM1 promotes neuroinflammation and inhibits neural regeneration after spinal cord injury through NF- κ B signaling. *Theranostics* 11, 4187–4206. doi: 10.7150/thno.49054
- Loreto, A., Angeletti, C., Gu, W., Osborne, A., Nieuwenhuis, B., Gilley, J., et al. (2021). Neurotoxin-mediated –potent activation of the axon degeneration regulator SARM1. *eLife* 10:e72823. doi: 10.7554/eLife.72823
- Lukacs, M., Gilley, J., Zhu, Y., Orsomando, G., Angeletti, C., Liu, J., et al. (2019). Severe biallelic loss-of-function mutations in nicotinamide mononucleotide adenylyltransferase 2 (NMNAT2) in two fetuses with fetal akinesia deformation sequence. *Exp. Neurol.* 320:112961. doi: 10.1016/j.expneurol.2019.112961
- Madisen, L., Zwingman, T. A., Sunkin, S. M., Oh, S. W., Zariwala, H. A., Gu, H., et al. (2010). A robust and high-throughput Cre reporting and characterization system for the whole mouse brain. *Nat. Neurosci.* 13, 133–140. doi: 10.1038/nn.2467
- Marion, C. M., McDaniel, D. P., and Armstrong, R. C. (2019). Sarm1 deletion reduces axon damage, demyelination, and white matter atrophy after experimental traumatic brain injury. *Exp. Neurol.* 321:113040. doi: 10.1016/j.expneurol.2019.113040
- Matsuoka, T., Ahlberg, P. E., Kassaris, N., Iannarelli, P., Dennehy, U., Richardson, W. D., et al. (2005). Neural crest origins of the neck and shoulder. *Nature* 436, 347–355. doi: 10.1038/nature03837
- Merlini, E., Coleman, M. P., and Loreto, A. (2022). Mitochondrial dysfunction as a trigger of programmed axon death. *Trends Neurosci.* 45, 53–63. doi: 10.1016/j.tins.2021.10.014
- Mo, W., and Nicolson, T. (2011). Both pre- and postsynaptic activity of Nsf prevents degeneration of hair-cell synapses. *PLoS One* 6:e27146. doi: 10.1371/journal.pone.0027146
- Oehlers, S. H., Cronan, M. R., Scott, N. R., Thomas, M. I., Okuda, K. S., Walton, E. M., et al. (2015). Interception of host angiogenic signalling limits mycobacterial growth. *Nature* 517, 612–615. doi: 10.1038/nature13967
- Osterloh, J. M., Yang, J., Rooney, T. M., Fox, A. N., Adalbert, R., Powell, E. H., et al. (2012). dSarm/Sarm1 is required for activation of an injury-induced axon death pathway. *Science* 337, 481–484. doi: 10.1126/science.1223899
- Preibisch, S., Saalfeld, S., and Tomancak, P. (2009). Globally optimal stitching of tiled 3D microscopic image acquisitions. *Bioinformatics* 25, 1463–1465. doi: 10.1093/bioinformatics/btp184
- Rondelli, A. M., Morante-Redolat, J. M., Bankhead, P., Vernay, B., Williams, A., and Carrillo-Barberá, P. (2023). AimSeg: A machine-learning-aided tool for axon, inner tongue and myelin segmentation. *bioRxiv [Preprint]* doi: 10.1101/2023.01.02.522533
- Sasaki, Y., Kakita, H., Kubota, S., Sene, A., Lee, T. J., Ban, N., et al. (2020). SARM1 depletion rescues NMNAT1-dependent photoreceptor cell death and retinal degeneration. *eLife* 9:e62027. doi: 10.7554/eLife.62027
- Schindelin, J., Arganda-Carreras, I., Frise, E., Kaynig, V., Longair, M., Pietzsch, T., et al. (2012). Fiji: An open-source platform for biological-image analysis. *Nat. Methods* 9, 676–682. doi: 10.1038/nmeth.2019
- Tian, W., Czopka, T., and López-Schier, H. (2020). Systemic loss of Sarm1 protects Schwann cells from chemotoxicity by delaying axon degeneration. *Commun. Biol.* 3:49. doi: 10.1038/s42003-020-0776-9
- Tsunoda, I. (2008). Axonal degeneration as a self-destructive defense mechanism against neurotropic virus infection. *Future Virol.* 3, 579–593. doi: 10.2217/174660794.3.6579
- Turkiew, E., Falconer, D., Reed, N., and Höke, A. (2017). Deletion of Sarm1 gene is neuroprotective in two models of peripheral neuropathy. *J. Peripher. Nerv. Syst.* 22, 162–171. doi: 10.1111/jns.12219
- Uccellini, M. B., Bardina, S. V., Sánchez-Aparicio, M. T., White, K. M., Hou, Y.-J., Lim, J. K., et al. (2020). Passenger mutations confound phenotypes of SARM1-deficient mice. *Cell Rep.* 31:107498. doi: 10.1016/j.celrep.2020.03.062
- van Rheenen, W., Shatunov, A., Dekker, A. M., McLaughlin, R. L., Diekstra, F. P., Pulit, S. L., et al. (2016). Genome-wide association analyses identify new risk variants and the genetic architecture of amyotrophic lateral sclerosis. *Nat. Genet.* 48, 1043–1048. doi: 10.1038/ng.3622
- Wu, T., Zhu, J., Strickland, A., Ko, K. W., Sasaki, Y., Dingwall, C. B., et al. (2021). Neurotoxins subvert the allosteric activation mechanism of SARM1 to induce neuronal loss. *Cell Rep.* 37:109872. doi: 10.1016/j.celrep.2021.109872
- Ye, J., Coulouris, G., Zaretskaya, I., Cutcutache, I., Rozen, S., and Madden, T. L. (2012). Primer-BLAST: A tool to design target-specific primers for polymerase chain reaction. *BMC Bioinformatics* 13:134. doi: 10.1186/1471-2105-13-134
- Zhu, C., Li, B., Frontzek, K., Liu, Y., and Aguzzi, A. (2019). SARM1 deficiency up-regulates XAF1, promotes neuronal apoptosis, and accelerates prion disease. *J. Exp. Med.* 216, 743–756. doi: 10.1084/jem.20171885